Ph.D Dissertation

Tunable Dual-Band Microwave Bandpass Filters With Wideband Harmonic Suppression

광대역 고조파 억제 특성을 갖는 가변 이중대역 마이크로파 대역통과 여파기

2013. 02. 22

Graduate School of
Chonbuk National University

Division of Electronics and Information Engineering

Girdhari Chaudhary

Tunable Dual-Band Microwave Bandpass Filters With Wideband Harmonic Suppression

광대역 고조파 억제 특성을 갖는 가변 이중대역 마이크로파 대역통과 여파기

2013. 02. 22

Graduate School of
Chonbuk National University

Division of Electronics and Information Engineering

Girdhari Chaudhary

Tunable Dual-Band Microwave Bandpass Filters With Wideband Harmonic Suppression

Academic Advisor: Professor Yongchae Jeong

A Dissertation Submitted In Partial Fulfillment of the
Requirements for the Degree
Doctor of Philosophy

2012. 09.24

Graduate School of
Chonbuk National University

Division of Electronics and Information Engineering

Girdhari Chaudhary

The Ph.D dissertation of Girdhari Chaudhary

is approved by

Chair, Professor, Hang-Geun Jeong
Chonbuk National University

Vice Chair, Professor, Hae-Won Son
Chonbuk National University

Professor, Gyu-Je Sung
Hankyong National University

Professor, Moon-Que Lee
University of Seoul

Advisor, Professor, Yongchae Jeong
Chonbuk National University

2012. 12.13

Graduate School of
Chonbuk National University

To my beloved family

ACKNOWLEDGEMENTS

TABLE OF CONTENTS

CHAPTER 1

CHAPTER 2

DESIGN OF DUAL-BAND BANDPASS FILTERS USING

NEW MAPPING FUNCTION

CHAPTER 3

DESIGN OF DUAL-BAND BANDPASS FILTER USING

DGS WITH CONTROLLABLE SECOND PASSBAND

CHAPTER 4

HARMONIC SUPPRESSED DUAL-BAND FILTERS WITH

TUNABLE PASSBANDS

CHAPTER 5

DUAL-BAND BANDPASS FILTER WITH

INDEPENDENTLY TUNABLE CENTER FREQUENCIES

AND BANDWIDTHS

CHAPTER 6

CONCLUSION AND FUTURE WORKS

LIST OF FIGURES

LIST OF TABLES

ABSTRACT

Girdhari Chaudhary

Division of Electronics and Information Engineering

The Graduate School

Chonbuk National University

In modern wireless communication systems, multi-band/multi-mode devices are becoming a major trend due to their ability to cover different communication standards and functionality with a single device. This trend demands the development of tunable and reconfigurable multi-band/multi-mode filters that constitute a key component in the radio frequency (RF) front-ends. This multi-band filter can select more than one band at same time or can cover the large frequency ranges using tunable multi-band bandpass filters (BPFs).

New challenges such as tunable multi-band passband response having a flexible center frequency as well as tunable bandwidths are being discovered in development and realization of multi-band microwave filters for different applications of wireless communication systems. With tunable passband frequency characteristics in filters, the harmonic bands which degrades the out-of passband characteristics, are also tuned. So the suppression of harmonics is one of the critical issues for tunable/multi-band filters.

The objective of this dissertation is the design and synthesis of planar transmission lines dual-band/tunable BPFs at microwave frequency ranges. The characteristics of designed filters such as passband center frequency, bandwidth, and/or selectivity, are electronically

tuned by a DC voltage control. The harmonic suppressed dual-band BPFs with tunable passbands based on defected ground structure (DGS) are also presented in this dissertation.

ABSTRACT IN KOREAN

요약

현대 무선 통신 시스템에서 하나의 기기로 서로 다른 통신규격이나 기능들을 수용할 수 있는 다중 대역 또는 다중 모드 기기들이 대세를 이루고 있다. 이러한 추세는 무선 주파수 전단부를 구성하는 핵심 소자인 조정 및 재구성 가능 다중 대역 또는 다중 모드 여파기 개발을 요구한다. 이 다중 대역 여파기는 동시에 하나 이상의 주파수 대역을 선택하거나 가변 다중 대역 통과 여파기를 사용하여 넓은 주파수 범위에서 주파수 선택을 가능하게 한다.

중심 주파수를 가변할 수 있을 뿐만 아니라 주파수 대역폭을 조정할 수 있는 다중 가변 통과 대역 응답과 같은 새로운 시도들은 다양한 무선 통신 시스템의 응용을 위한 다중 대역 마이크로파 여파기의 개발 및 구현으로 나타나게 된다. 다중 가변 여파기의 주파수 선택 특성은 통과 대역 외부의 여파기 특성을 열화시키는 고조파 주파수 대역 역시 가변시킨다. 따라서 고조파의 억제가 가변 다중 대역 여파기의 중요한 설계 항목 중 하나이다.

이 논문의 목적은 초고주파 대역에서 평면형 전송 선로를 이용한 가변 이중대역 대역통과 여파기의 설계 및 분석이다. 통과 대역의 중심 주파수, 대역폭 또는 선택도와 같이 설계된 여파기의 특성은 DC 전압 제어를 통해 전자적으로 조정된다. 결함 접지 구조(DGS)를 이용한 가변 이중대역 대역통과 여파기의 고조파 억제 특성도 본 논문에서 제시된다.

ABBREVIATIONS

ADS	advanced design system
BPF	band pass filter
CPW	coplanar waveguide
CSSR	complement split ring resonator
DC	direct current
DGS	defected ground structure
FBW	fractional bandwidth
EM	electromagnetic
GPS	global positioning system
HFSS	high frequency structure simulator
IF	intermediate frequency
IIP	inter-modulation intercept point
I/O	input/output
LNA	low-noise amplifier
LPF	low pass filter
LTCC	low temperature co-fired ceramic
LTE	long term evolution
MEMS	micro-electromechanical system
MLR	meandered loop resonator
PA	power amplifier
RF	radio frequency

RX   receiver

SIR   stepped impedance resonator

SIW   substrate integrated waveguide

SLR   stub-loaded resonator

TX   transmitter

WCDMA   wideband code division multiple access

WiMax   world-wide interoperability for microwave access

WLAN   wireless local area network

YIG   yittrium-iron-garnet

CHAPTER 1

1.0 Introduction

In the process of rapid evolution into microwave wireless communication, the demand of multi-band/multi-mode functional microwave systems that support various modern services such as voice, data, and multi-media have been increased rapidly. Therefore, this demand requires a wide variety of analog circuits containing several power amplifiers (PAs), filters, oscillators, antennas etc., for each specific frequency application. BPFs are important components of wireless systems as they enable band selection and eliminate interference between the channels in RF transceivers. In the multi-band communication systems, a single BPF generally can not fulfill the filtering requirements for all of bands. Therefore, the filter-bank followed by switching elements are used which results a large circuit size and an increased complexity of systems.

The ideal solution is to develop tunable multi-band filters for replacing the filter bank without degradation in filter performance as shown in Fig. 1.1. An electronically tunable multi-band filters have an control circuit to adjust their characteristics such as center frequency, bandwidth, and/or selectivity in a predefined and controlled manner, replacing the need of multiple channels, improving overall system reliability, reducing size, weight, complexity and cost.
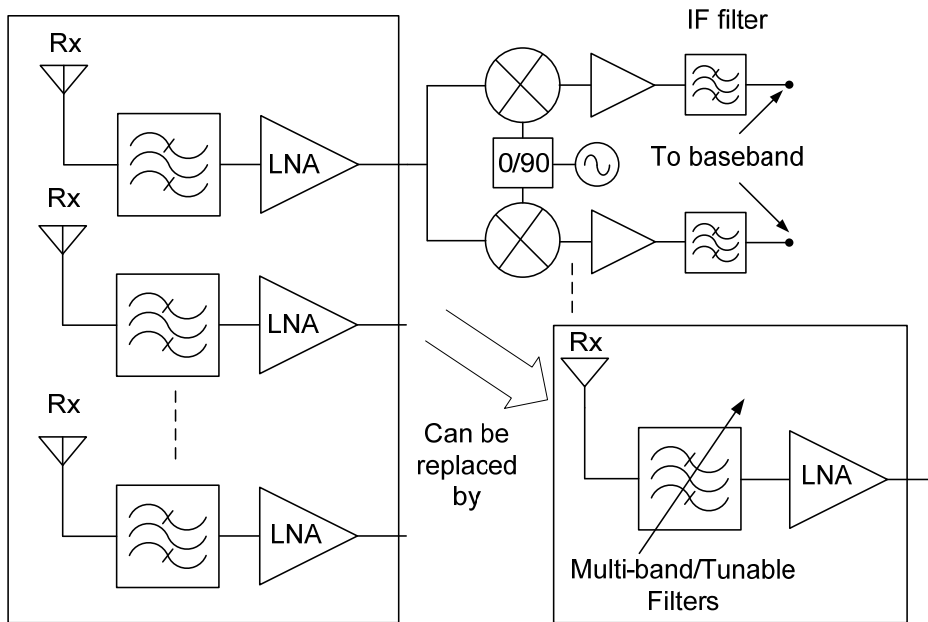
(a)
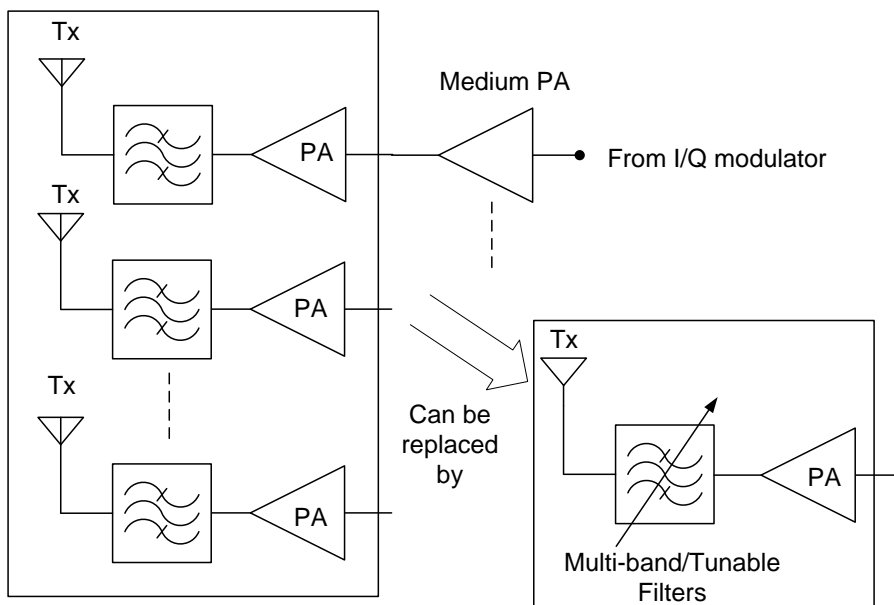
(b)

Fig. 1.1 Block diagram of tunable multi-band wireless communication system (a) receiver and (b) transmitter.

1.1 Literature Review

Extensive researches on the design of dual-band BPFs have been presented [1]-[22]. One of simplest methods to design the dual-band BPF is by connecting two different BPFs in parallel to obtain the dual-band characteristics [1]. Another approach is to insert a narrowband bandstop filter into the broadband BPF to create the dual-band characteristics using Z-transform synthesis [2]. Because two different filters are used, the sizes of these dual-band BPFs are comparatively large.

Another straightforward approach is to optimize both the physical dimensions and structures of dual-band BPF to meet the required dual-band BPF specifications using optimization techniques such genetic algorithms [3] and annealing algorithms [4]. A synthesis method for a self-equalized dual-band BPF has been presented in [5]. A dual-band BPF of canonical structure with a dual-mode have been designed and realized in [6]. These methods are based on a numerical optimization technique in the filter synthesis process, which requires a long optimization time.

In order to avoid the optimization technique, a method called the frequency transformation technique has been presented in designing the dual-band BPF. One of the frequency transformations presented in [7] is used for designing the asymmetric dual-band BPF. The BPF with dual-passband characteristics and associated frequency transformations are presented in [8], which requires the optimization process to achieve the equiripple in the passband. A synthesis technique for symmetric dual-band BPF using the frequency transformation is

presented in [9]. However, this transformation can not provide the equiripple response in the passband.

Using a successive frequency transformation, the design of dual-band BPF is presented in [10]-[12]. Although the center frequencies of passbands can be chosen separately, the design process requires the same fractional bandwidths (FBWs) for the first and second passbands. The design of wide dual-band passband BPF using the frequency mapping is presented in [13].

A lumped element dual-band BPF implemented with a low temperature co-fired ceramic (LTCC) technology is presented in [14]. The size of the filter is compact, but the out-of-band characteristics are worse. A design methodology for dual-band BPF using an artificial lumped-element coplanar waveguide (CPW) is presented in [15].

Currently, the coupling matrix method is widely used for designing dual-band or multi-band microwave filters. One method is to find a suitable coupling matrix such that the dual-band or multi-band response is created by placing the transmission zeros within the wideband BPF [16]-[17]. This method requires an initial estimation of the coupling coefficients because of the optimization process. In addition, the implementation requires sufficiently large coupling coefficients to meet the overall specifications of dual-band BPF.

Recently, multi-mode resonators such as stepped impedance resonators (SIRs), stub loaded SIRs, meander-loop resonators (MLR) and complement split-ring resonator (CSRR) DGS were widely used for designing dual-band BPFs by utilizing higher resonant modes of the resonator [18]-[21]. The resonant modes of

the SIR can be controlled by the characteristic impedances of the high and low sections of the resonator. However, these approaches encounter difficulties when adjusting for the coupling coefficients between neighboring resonators in order to meet the dual-band specifications simultaneously. Additionally, in some cases, dual-band transformers are required to match the port impedance [21], which increases the implementation area. In [22], dual-band BPF with controllable bandwidths has been presented. However, these require some complex and time consuming mathematical calculation to find the desired element values of filter.

Several types of tunable filters have also been presented in the literature using different technologies, topologies, and tuning mechanism [23]-[50]. Most tunable filters described in literature fall into three basic types: mechanically tunable, magnetically tunable, and electronically tunable filters [23]. Mechanically tunable filters have large power handling capability and low insertion loss. However, their low tuning speed and large size prevent the possibility of using them in modern communication system.

Yittrium-Iron-Garnet (YIG) filters are example of magnetically tunable filters [24]-[25]. The filter uses ferromagnetic resonators and gyromagnetic coupling. The tuning is done utilizing the variation in the ferromagnetic resonant frequency of YIG spheres by applying an external DC magnetic field. YIG filters provides advantages of multi-octave tuning range, spurious-free response, low insertion loss and high quality factor resonators. However, YIG filters are not plannar structure which limits their use in modern wireless communication systems.

Electronically tunable filters are mainly based micro-electromechanical system (MEMS) devices [26]-]29], [49], ferroelectric devices/capacitors [30]-[31], piezoelectric transducer [32], p-i-n diodes [33] and semiconductor varactor diodes [34]-[39], [47]-[48], [50]. The RF-MEMS devices are also widely used to design tunable filters due to their high quality factor (Q) and high linearity. However, the high cost and maturity of RF-MEMS technology limits their application in design of tunable devices.

The semiconductor varactors are widely used in designing tunable BPFs due to high tuning speed and reliability. Hunter *et al.* [34] and Kim *et al.* [35] demonstrated a varactor tuned combline filter. Brown *et al.* [36] reported a four-pole varactor tuned interdigital filter. Park *et al.* [37] demonstrated two-pole tunable filters with the predefined bandwidth characteristics. Tang *et al.* [38] designed the tunable BPF using dual-mode resonators. In order to improve the selectivity of BPFs, the filter with transmission zeros was presented in [39]-[40]. In [41], ferroelectric capacitors were used to design tunable bandpass filters for *K*a and *U*-band applications. In [42], a substrate integrated waveguide (SIW) cavity filter with wide tuning range is presented. However, none of the above work addressed the design of tunable dual-passbands simultaneously.

There have been some attempts to design the tunable dual-band filters [43]-[45]. However, these works focused on the design of fixed first passband and tunable second passband. None of the above referenced works focused on design of tunable dual-passbands simultaneously. Djoumessi *et al.* [46] demonstrated the varactor

tuned quarter-wavelength dual-band BPF which had a huge circuit size, large number of varactor diodes and biasing circuits.

1.2   Dissertation Objectives and Organization

The main objective of this dissertation is to explore novel multi-band/tunable BPF designs for multifunctional wireless systems. Firstly, dual-band BPF with arbitrary bandwidths are explored in this work. A purely lumped element approach is taken to extract circuit element values of proposed filter and implemented with distributed transmission lines utilizing circuit conversion technique.

One of points that seems to be lacking from current publication is the design of tunable multi-band BPFs. As part of the contribution of this work, the design of tunable dual-band BPF with independently tunable center frequency and bandwidths are presented in this thesis. The characteristics of designed filters such as center frequency, bandwidth and selectivity are electronically adjusted by a DC control voltage. For that, it was investigated the integration of commercially available components such as varactor diodes for applications in microwave frequencies with transmission line filters. Detail analytical equations are presented explaining the design methods which are verified through circuit simulations and experimental results.

With tunable passband frequency characteristic in the tunable filters, the harmonic bands which degrade the out-of passband characteristics, are also tuned. So, the suppression of harmonics is one of the critical issues for the tunable filters. This issue has rarely been addressed in the design of tunable dual-band filters in the

previous publications. As another contribution of this thesis, a harmonic suppressed tunable dual-band BPF is presented. The proposed filter shows a rejection level of 20 dB up to more than 10 times of highest center frequency of the second passband.

The rest of this dissertation is organized as follows. Chapter 2 describes the design of dual-band BPF with the tunable bandwidths using new mapping function. The circuit conversion technique is used to implement the proposed filter with distributed transmission line at microwave frequencies.

Chapter 3 presents the design of dual-band BPF with the tunable second passband using the DGS. In this chapter, the characteristics of stub-loaded resonator (SLR) and variable characteristic impedance transmission line using the DGS are investigated and applied to the design of dual-band BPF.

Chapter 4 is devoted to design a harmonic suppressed dual-band BPF with tunable passbands. In this chapter, the characteristics of dual-mode resonator based on the transmission line loaded with varactor diodes are investigated and applied to the design of tunable dual-band BPF. The band-rejection characteristics of the DGS are utilized to suppress the harmonics of tunable filters over a broad frequency range.

Chapter 5 describes the design of dual-band BPF with independently tunable center frequency and bandwidths. The characteristics of dual-mode resonators are described based on even-and odd-mode analysis.

Finally, Chapter 6 summarizes the contributions of the dissertation and provides ideas for future research in this area.

CHAPTER 2

DESIGN OF DUAL-BAND BANDPASS FILTERS USING NEW MAPPING FUNCTION

In this chapter, a novel design method for the dual-band BPF with arbitrary bandwidths based on a simple frequency mapping function is proposed and its analytical design equations are also derived. The circuit conversion techniques are employed for implementation with distributed transmission line. To validate the proposed dual-band BPF with arbitrary bandwidths, the LTCC transmission line as well as microstrip lines are used, respectively. The two types of designed dual-band BPF have the same and significantly different FBWs, respectively.

2.1 Design Theory

Fig. 2.1 shows n^{th} order prototype low pass filters (LPFs). The element values of LPF can be obtained using the well known formula given in [51].
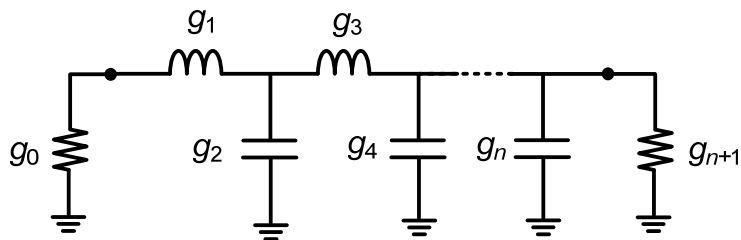
(a)
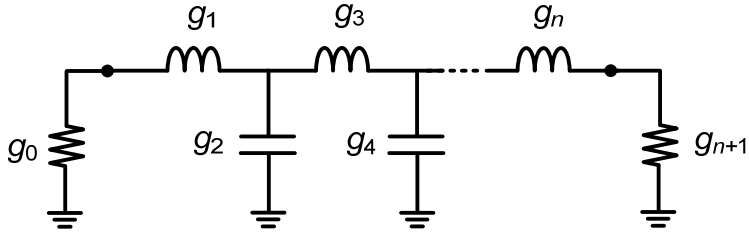
(b)

Fig. 2.1. Low-pass filter prototype elements : (a) n is even and (b) n is odd.

Fig. 2.2 shows typical Chebyshev LPF attenuation characteristics. In this case, L_{Ar} is the maximum insertion loss ripple in the passband, while ω'_1 is the passband edge angular frequency.
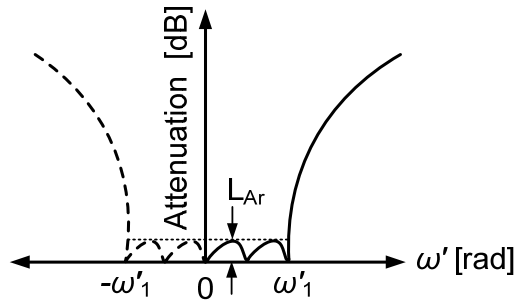
Fig. 2.2.   Typical attenuation characteristic of Chebyshev low-pass filter.

Fig. 2.3 shows the circuit diagrams of the proposed dual-band BPF and its attenuation characteristics. The frequency response characteristics of the proposed dual-band BPF can be obtained by mapping the frequency response of LPF. The frequency $-\omega'_1$ of LPF is mapped to ω_1 and ω_3 whereas the frequency ω'_1 is mapped to ω_2 and ω_4, respectively, where ω_1 and ω_2 are the lower and the upper edge

16

angular frequencies of the first passband and ω_3 and ω_4 are the lower and the upper edge angular frequencies of the second passband, as shown in Fig. 2.3(c).

The series-branch circuit elements of the proposed dual-band BPF can be obtained from the series circuit elements of LPF. The input impedance of the series elements of LPF is given as:

$$Z'_{\text{in\_series}} = j\omega' g_k = jX'_{\text{series}} \qquad (2.1)$$
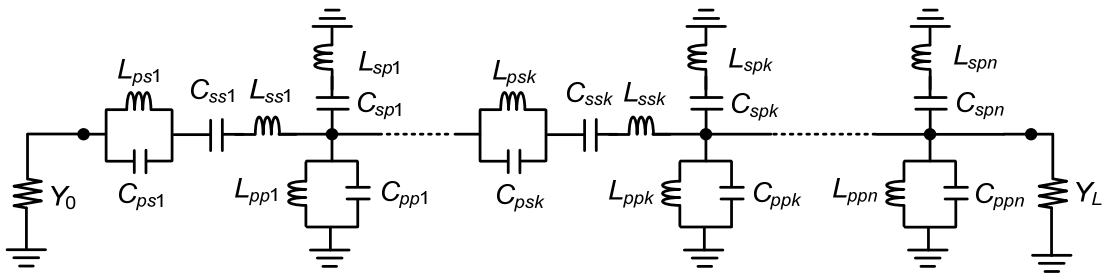
(a)
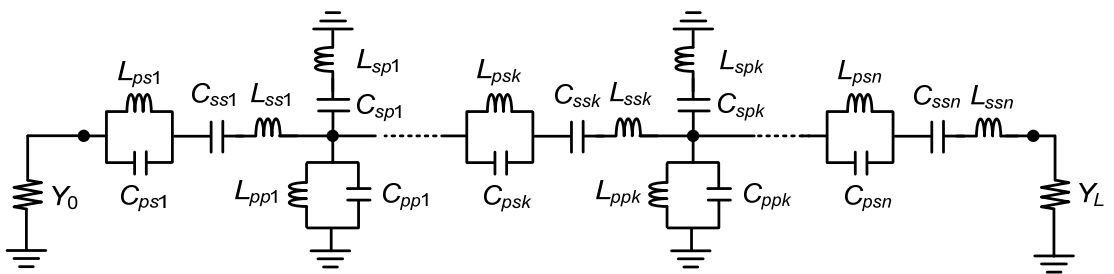
(b)
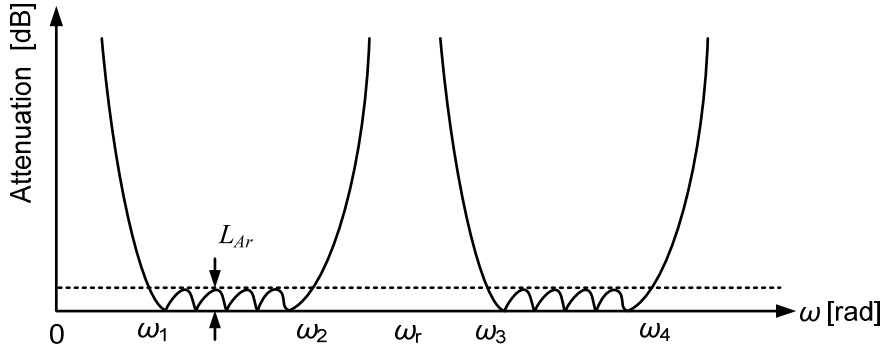
(c)

Fig. 2.3. The circuit elements of the proposed dual-band BPF : (a) n is even, (b) n is odd, and (c) attenuation characteristics of Chebyshev dual-band BPF.

Similarly, considering the series-branch elements of the proposed dual-band BPF, the input impedance is given as:

$$Z_{in\_series} = j\left(\frac{\omega L_{psk}}{1 - \frac{\omega^2}{\omega_{ops}^2}} - \frac{1 - \frac{\omega^2}{\omega_{oss}^2}}{\omega C_{ssk}} \right) = jX_{series} \qquad (2.2)$$

The values of ω_{ops} and ω_{oss} are given as:

$$\omega_{ops} = \frac{1}{\sqrt{L_{psk}C_{psk}}} \qquad (2.3)$$

$$\omega_{oss} = \frac{1}{\sqrt{L_{ssk}C_{ssk}}} \qquad (2.4)$$

Fig. 2.4 shows the reactance characteristics of the series-branch of the LPF and the proposed dual-band BPF.

18
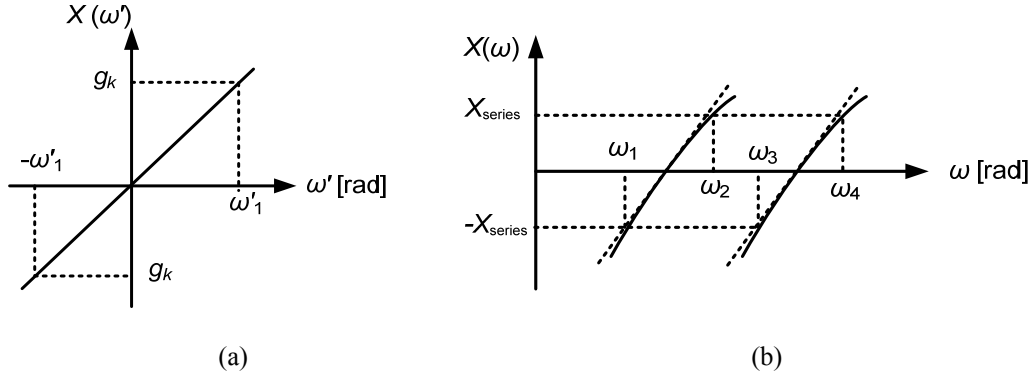
Fig. 2.4. The reactance characteristics of the series branch : (a) low-pass filter and (b) dual-band BPF.

From the reactance characteristics shown in Fig. 2.4, it can be inferred that the sum of the reactance at ω_1, ω_2 and at ω_3, ω_4 is zero, respectively. Similarly, the reactance at ω_1 is equal to the reactance at ω_3 and the reactance at ω_2 is equal to the reactance at ω_4, as indicated in (2.5)-(2.8).

$$X_{series}\left(\omega_1\right) + X_{series}\left(\omega_2\right) = 0 \tag{2.5}$$

$$X_{series}\left(\omega_3\right) + X_{series}\left(\omega_4\right) = 0 \tag{2.6}$$

$$X_{series}\left(\omega_1\right) = X_{series}\left(\omega_3\right) \tag{2.7}$$

$$X_{series}\left(\omega_2\right) = X_{series}\left(\omega_4\right) \tag{2.8}$$

From (2.2) and (2.5)-(2.8), the mapping function is given as:

$$L_{psk}C_{ssk} = \frac{A_1 + A_2}{B_1 + B_2} = \frac{A_3 + A_4}{B_3 + B_4} = \frac{A_1 - A_3}{B_1 - B_3} = \frac{A_2 - A_4}{B_2 - B_4} = \alpha \tag{2.9}$$

The value of A_i and B_i are given as:

$$A_i = \frac{1 - \dfrac{\omega_i^2}{\omega_{oss}^2}}{\omega_i} \tag{2.10}$$

$$B_i = \frac{\omega_i}{1 - \dfrac{\omega_i^2}{\omega_{ops}^2}} , \quad i = 1, 2, 3, 4 \tag{2.11}$$

Using (2.1), (2.2), and (2.9) for $\omega' = \omega'_1 = 1$ and $\omega = \omega_2$, the series-branch circuit element values of the proposed dual-band BPF can be obtained.

$$L_{psk} = \frac{g_k Z_0}{\left(\dfrac{\omega_2}{1 - \dfrac{\omega_2^2}{\omega_{ops}^2}} - \dfrac{1 - \dfrac{\omega_2^2}{\omega_{oss}}}{\omega_2 \alpha} \right)} \tag{2.12}$$

$$C_{psk} = \frac{1}{\omega_{ops}^2 L_{psk}} \tag{2.13}$$

$$C_{ssk} = \frac{\alpha}{L_{psk}} \tag{2.14}$$

$$L_{ssk} = \frac{1}{\omega_{oss}^2 C_{ssk}}, \quad k = 1, 2, \cdots n \tag{2.15}$$

Where Z_0 is the termination source impedance.

Similarly, the shunt-branch circuit elements of the proposed dual-band BPF can be obtained from the shunt-branch circuit elements of LPF. The input admittance of the shunt-branch elements of LPF is given as.

$$Y'_{in\_shunt} = j\omega' g_k = jB'_{shunt} \tag{2.16}$$

The input admittance of the shunt-branch elements of the proposed dual-band BPF is given as:

$$Y_{in\_shunt} = j\left(\frac{\omega C_{spk}}{1 - \dfrac{\omega^2}{\omega_{osp}^2}} - \frac{1 - \dfrac{\omega^2}{\omega_{opp}^2}}{\omega L_{ppk}} \right) = jB_{shunt} \tag{2.17}$$

The values of ω_{osp} and ω_{opp} are given as:

$$\omega_{osp} = \frac{1}{\sqrt{L_{spk}C_{spk}}} \tag{2.18}$$

$$\omega_{opp} = \frac{1}{\sqrt{L_{ppk}C_{ppk}}} \tag{2.19}$$

Fig. 2.5 shows the susceptance characteristics of the shunt-branch of the LPF and the proposed dual-band BPF.

(a) (b)
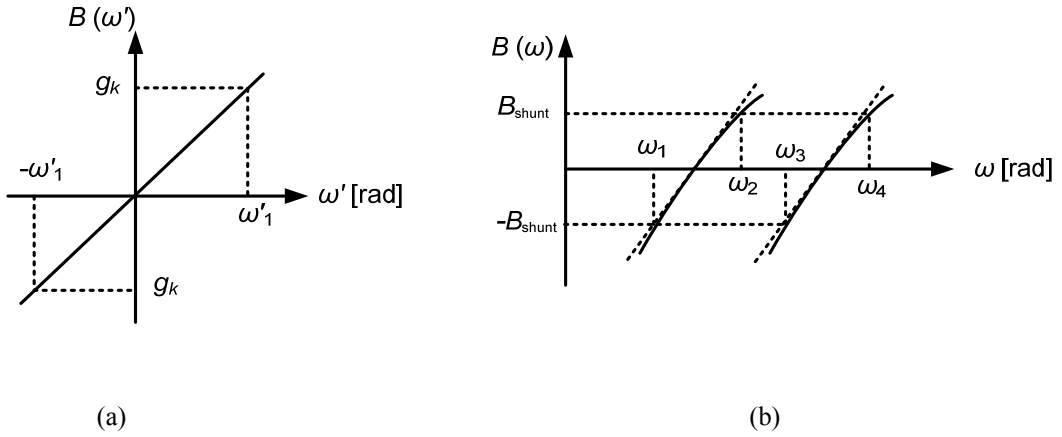
Fig. 2.5. Susceptance characteristics of shunt branch : (a) low-pass filter and (b) dual-band BPF.

Similarly to the series element case, from the susceptance graph of the dual-band BPF, the susceptance equations can be written as:

$$B_{shunt}(\omega_1) + B_{shunt}(\omega_1) = 0 \tag{2.20}$$

$$B_{\text{shunt}}\left(\omega_3\right) + B_{\text{shunt}}\left(\omega_4\right) = 0 \tag{2.21}$$

$$B_{\text{shunt}}\left(\omega_1\right) = B_{\text{shunt}}\left(\omega_3\right) \tag{2.22}$$

$$B_{\text{shunt}}\left(\omega_2\right) = B_{\text{shunt}}\left(\omega_4\right) \tag{2.23}$$

Using (2.17) and (2.20)-(2.23), the mapping function is given as:

$$L_{ppk}C_{ppk} = \frac{C_1 + C_2}{D_1 + D_2} = \frac{C_3 + C_4}{D_3 + D_4} = \frac{C_1 - C_3}{D_1 - D_3} = \frac{C_2 - C_4}{D_2 - D_4} = \beta \tag{2.24}$$

The values of C_i and D_i are given as:

$$C_i = \frac{1 - \dfrac{\omega_i^2}{\omega_{opp}^2}}{\omega_i} \tag{2.25}$$

$$D_i = \frac{\omega_i}{1 - \dfrac{\omega_i^2}{\omega_{osp}^2}} \ , \ i = 1, 2, 3, 4 \tag{2.26}$$

The values of ω_{opp} and ω_{osp} have already been given by (2.18) and (2.19), respectively. Using (2.16), (2.17) and (2.24) for $\omega' = \omega'_1 = 1$ and $\omega = \omega_2$, the shunt-branch circuit element values of the proposed dual-band BPF can be obtained.

$$C_{spk} = \frac{g_k}{\left(\dfrac{\omega_2}{1 - \dfrac{\omega_2^2}{\omega_{osp}^2}} - \dfrac{1 - \dfrac{\omega_2^2}{\omega_{opp}^2}}{\omega_2 \beta} \right) Z_0} \tag{2.27}$$

$$L_{spk} = \frac{1}{\omega_{osp}^2 C_{spk}} \tag{2.28}$$

$$L_{ppk} = \frac{\beta}{C_{spk}} \tag{2.29}$$

$$C_{ppk} = \frac{1}{\omega_{osp}^2 L_{ppk}}, \quad k = 1, 2, \cdots n \tag{2.30}$$

The circuits of the proposed dual-band BPF shown in Fig. 2.3 consist of both series and parallel LC resonators circuits in the series and shunt-branches. These circuits are difficult to implement using only lumped elements at the microwave frequencies. In order to implement the above circuits of the proposed dual-band BPF with a planar transmission line, the circuit conversion technique is employed. By applying the circuit conversion technique, the series-branch elements are replaced with admittance inverters (*J*-inverters), which are shown in Fig. 2.6(a). For odd values of *i*, the circuit elements of Fig. 2.6(a) are given by (2.31)-(2.34).

$$C_{a1} = J_{01}^2 L_{ss1} \quad , L_{a1} = \frac{C_{ss1}}{J_{01}^2} \tag{2.31}$$

$$L_{b1} = \frac{C_{ps1}}{J_{01}^2} \quad , \quad C_{b1} = J_{01}^2 L_{ps1} \tag{2.32}$$

$$C_{ai} = \frac{J_{01}^2 \cdots J_{l+2,l+3}^2}{J_{12}^2 \cdots J_{m+2,m+3}^2} L_{ssi} \quad , L_{ai} = \frac{J_{12}^2 \cdots J_{m+2,m+3}^2}{J_{01}^2 \cdots J_{l+2,l+3}^2} C_{ssi} \tag{2.33}$$

$$L_{bi} = \frac{J_{12}^2 \cdots J_{m+2,m+3}^2}{J_{01}^2 \cdots J_{l+2,l+3}^2} C_{psi} \ , \ C_{bi} = \frac{J_{01}^2 \cdots J_{l+2,l+3}^2}{J_{12}^2 \cdots J_{m+2,m+3}^2} L_{psi} \ (2.34)$$

Where the values of l and m are given as (2.35).

$$l = 0,1,\cdots,\frac{i-3}{2}, \ m = 1,2,\cdots\frac{i-3}{2}@ \ i = 1,3,\cdots,n \qquad (2.35)$$

When the value of i is even, the circuit elements of Fig. 2.6(a) are given by (2.36)-(2.37).

$$C_{ai} = \frac{J_{12}^2 \cdots J_{l+2,l+3}^2}{J_{01}^2 \cdots J_{l+1,l+2}^2} C_{ppi}, \ L_{ai} = \frac{J_{01}^2 \cdots J_{l+1,l+2}^2}{J_{12}^2 \cdots J_{l+2,l+3}^2} L_{ppi} \qquad (2.36)$$

$$C_{bi} = \frac{J_{12}^2 \cdots J_{l+2,l+3}^2}{J_{01}^2 \cdots J_{l+1,l+2}^2} L_{spi}, \ L_{bi} = \frac{J_{01}^2 \cdots J_{l+1,l+2}^2}{J_{12}^2 \cdots J_{l+2,l+3}^2} L_{spi} \qquad (2.37)$$

Where the value of l in this case is given as (2.38)

$$l = 1,2,\cdots,\frac{i-2}{2} \ @ \ i = 2,4,\cdots,n \qquad (2.38)$$

The circuit shown in Fig. 2.6(a) consists of both the series and parallel LC resonators in the shunt-branch. The parallel LC resonator can be replaced with the series LC resonator by utilizing the J-inverter and the circuit conversion technique. The modified circuit, which consists of only the series LC resonators and J-inverters, are shown in Fig. 2.6(b). The circuit elements shown in Fig. 2.6(b) are given as:

$$J_{xi} = \sqrt{\frac{C_{ai}}{L_{x_i}}} = \sqrt{\frac{C_{xi}}{L_{a_i}}} \quad i = 1,2,\cdots,n \qquad (2.39)$$
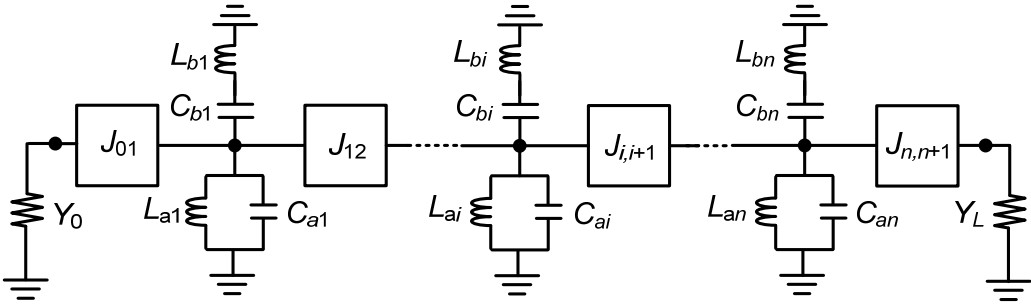
(a)
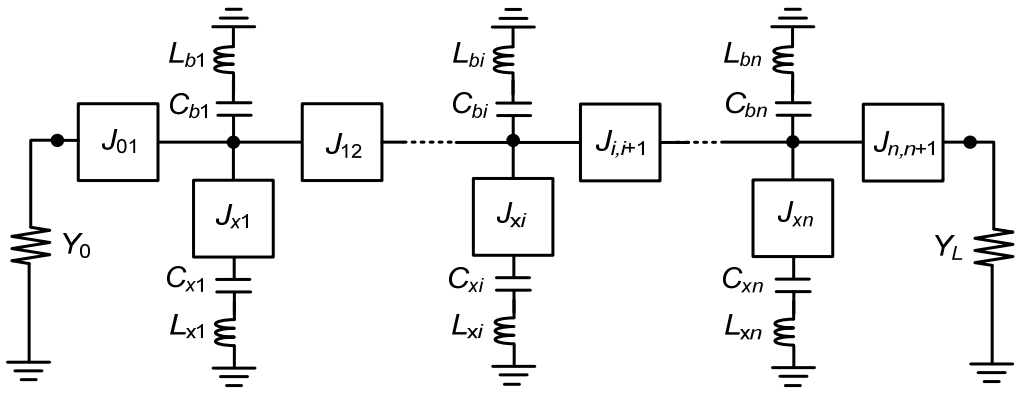
(b)

Fig. 2.6. Circuit of proposed dual-band BPF with (a) *J*-inverters, series and shunt LC resonator circuits and (b) *J*-inverter and only series LC resonators.

Theoretically, the chosen *J*-inverter values can be selected arbitrarily. However, in practice, *J*-inverter values should be chosen such that its physical dimensions can be realized without any difficulties. Introducing flexibility in the choice of *J*-inverter values allows the designer more freedom in the design and realization of the proposed dual-band BPFs.

2.2   LTCC Filter Implementation

In order to validate the proposed structure shown in Fig. 2.6(a) obtained from the novel frequency mapping function, two types of filters have been designed, simulated and measured with LTCC technology. The BPFs have been fabricated on a substrate of RN2 with a dielectric constant of 7.8 and a loss tangent of 0.003. The *J*-inverters are implemented with a quarter-wavelength transmission line [48] at the frequency $f_{or} = (f_{01}f_{02})^{0.5}$, where $f_{01} = (f_1f_2)^{0.5}$ is the geometric mean of the first passband edge frequencies (f_1, f_2) and $f_{02} = (f_3f_4)^{0.5}$ is the geometric mean of the second passband edge frequencies (f_3, f_4). Similarly, the series and parallel LC resonators in the shunt-branch are implemented with the open-stub and short-stub quarter-wavelength transmission line with characteristic impedances Z_o and Z_s Ω, at f_{oss} and f_{osp}, respectively. The 3-D structure and associated side-view of the designed LTCC BPF are shown in Fig. 2.7. The simulation utilized the Advanced Design System (ADS) 2009 of Agilent and the full-wave electromagnetic (EM) simulator HFSS v11 of Ansoft.
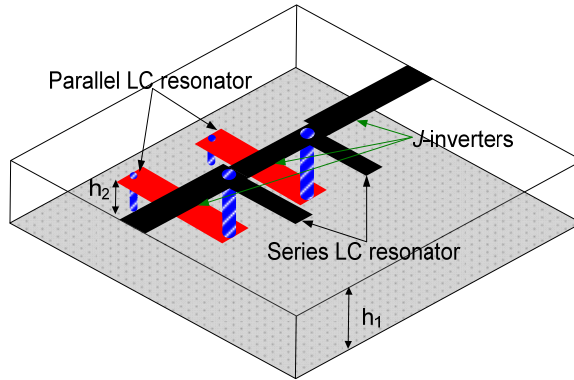
(a)
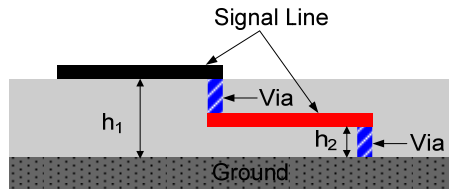
(b)

Fig. 2.7. Designed LTCC dual-band BPF: (a) 3-D structure and (b) side-view (h_1=1.3, h_2= 0.2, [mm]).

2.2.1 Dual-Band Filter With Same Fractional Bandwidths

The Filter I bandwidth specification is chosen with almost the same FBWs. The frequencies are specified as: f_1=2.11 GHz, f_2=2.17 GHz, f_3=3.45 GHz and f_4=3.55 GHz, where the FBW of the first and second passband are Δ_1=2.80 % and Δ_2=2.85 %, respectively. The calculated values of f_{oss} (or f_{opp}) and f_{ops} (or f_{osp}) are 2.7427 GHz and 2.7303 GHz, respectively. The prototype elements of the second-order Chebyshev filter with the passband ripple (ε) of 0.01 dB are as : g_0=1, g_1=0.4488, g_2=0.4077, and g_3=1.1007.

The calculated element values of the circuit shown in Fig. 2.6(a) are given as : $J_{01}=J_{23}=0.0147$, $J_{12}=0.0113$, $C_{a1}=C_{a2}=4.8276$ pF, $L_{a1}=L_{a2}=0.6975$ nH, $C_{b1}=C_{b2}=1.1935$ pF, $L_{b1}=L_{b2}=2.8471$ nH, $Z_s= 9.44$ Ω and $Z_o= 62.18$ Ω.

The short stub resonators have relatively too low characteristic impedances, making them difficult to implement in microstrip lines. This is because low impedance requires a very large width that is even larger than the length of transmission line. The solution to this issue involves utilization of LTCC technology, where the low and the high impedance transmission lines can be implemented within a practical width range, by controlling the height (h_2 and h_1) of the substrate layers.

Fig. 2.8 shows the simulation and measurement results for Filter I. There is good agreement between the simulation and measurement results except for a slight frequency shift in the measurement due to via misalignment during the LTCC manufacturing process.
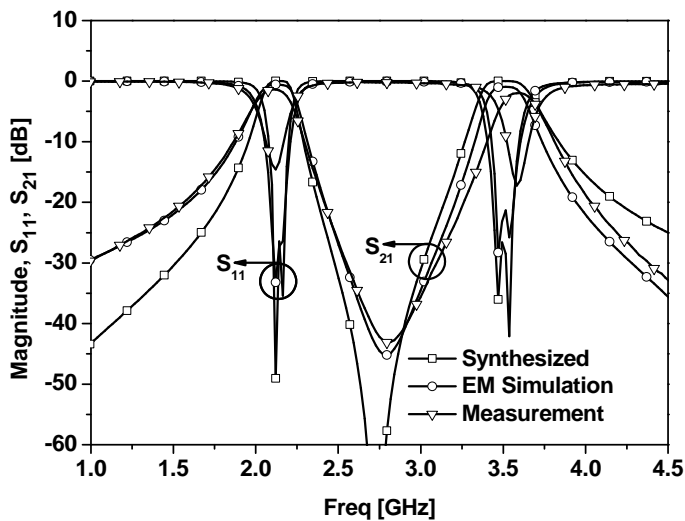
Fig. 2.8. Simulated and measurement results of fabricated LTCC Filter I.

The measured insertion losses are 1.31 dB and 1.92 dB at frequencies of 2.12 GHz and 3.59 GHz, respectively. Similarly, the measured return losses are 15.3 dB and 17.98 dB at these frequencies. The bandwidths at the first and second passbands are 66.8 MHz and 96.8 MHz, for which the FBWs are 3.02 % and 2.96 %, respectively.

2.2.2 Dual-Band Filter With Different Fractional Bandwidths

The specifications for Filter II is chosen with different FBWs. The frequencies are specified as: f_1=3.4 GHz, f_2=3.6 GHz, f_3=5.15 GHz and f_4=5.25 GHz, for which the FBW of the first and second passband are Δ_1=5.71% and Δ_2=1.92%, respectively. The prototype elements of a second-order Chebyshev LPF with the passband ripple (ε) of 0.01 dB are the same as Filter I. The calculated values of f_{oss} (or f_{opp}) and f_{ops} (or f_{osp}) are 3.8693 GHz and 4.7016 GHz, respectively. The calculated element values of the circuit shown in Fig. 2.6(a) are given as : J_{01}=J_{23}=0.0185, J_{12}=0.0179, C_{a1}=C_{a2}=4.0825 pF, L_{a1}=L_{a2}=0.4144 nH, C_{b1}=C_{b2}= 0.4029 pF, L_{b1}=L_{b2}=2.8442 nH, Z_s=7.91 Ω, and Z_o=106.98 Ω.

Fig. 2.9 shows the simulation and measurement results of Filter II. The measured insertion losses are 1.01 dB and 1.39 dB at the frequencies of 3.47 GHz and 5.36 GHz, respectively. Similarly, the measured return losses are 18.35 dB and 21.79 dB at these frequencies. The bandwidths at the first and second passbands are 192.1 MHz and 96.8 MHz, respectively, for which the FBWs are 5.53 % and 1.81 %, respectively.
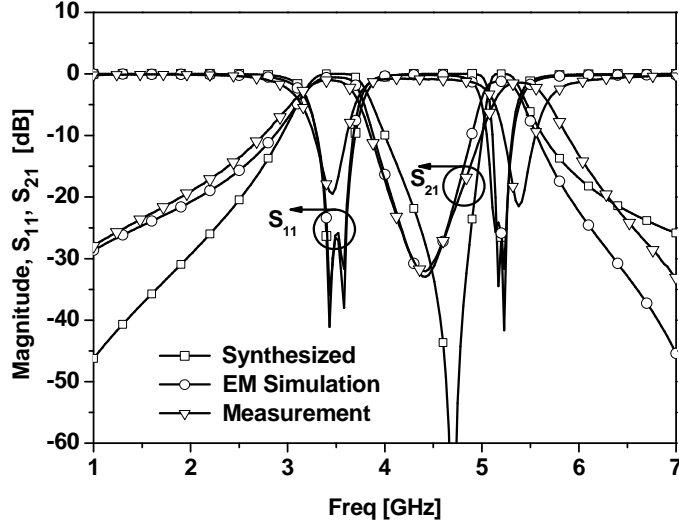
Fig. 2.9. Simulated and measurement results of fabricated LTCC Filter II.

2.3 Microstrip Lines Filter Implementation

In order to validate the proposed structure shown in Fig. 2.6(b) obtained from the novel frequency mapping function, another two types of BPFs with microstrip transmission lines have been designed, simulated and measured. The filters are fabricated on the Rogers RT/duroid 5880 substrate with a dielectric constant (ε_r) of 2.2 and a thickness (h) of 31 mils.

2.3.1 Dual-Band Filter With Same Fractional Bandwidths

The specification of the Filter III is the same as for Filter I in the previous section. The calculated values of elements shown in Fig. 2.6(b) for n=2 are $J_{01}=J_{23}=0.018$, $J_{12}=0.0174$, $J_{x1}=J_{x2}=0.037$, $L_{b1}=L_{b2}=1.8590$ nH, $C_{b1}=C_{b2}=1.8290$ pF, $L_{x1}=L_{x2}=5.4012$ nH, $C_{x1}=C_{x2}=0.6234$ pF. The physical layout and dimensions of Filter III shown in Fig. 2.10(a) are $W_{01}=2.4$, $l_{01}=19$, $W_{12}=2.1$, $l_{12}=18.2$, $W_x=1$,

l_x=19.5, W_1=2.9, L_1=18, W_b=2.2, l_b=18.4 mm, respectively.

Fig. 2.10(b) shows the simulation and measurement results of Filter III. The measurement and simulation results are in good agreement. The measured in-band insertion losses are 0.9 dB and 1.2 dB at 2.14 GHz and 3.5 GHz, respectively. The return loss at 2.11-2.17 GHz and 3.45-3.55 GHz in the first and second passband respectively, is greater than 21 dB. The measured bandwidths at the first and second passbands are 68.7 and 93.7 MHz, respectively, for which the FBWs are 2.92 % and 2.72 %, respectively. The attenuation is greater than 20 dB at frequencies of 2.6-3.25 GHz between the two passbands, which provides a good level of isolation between them.
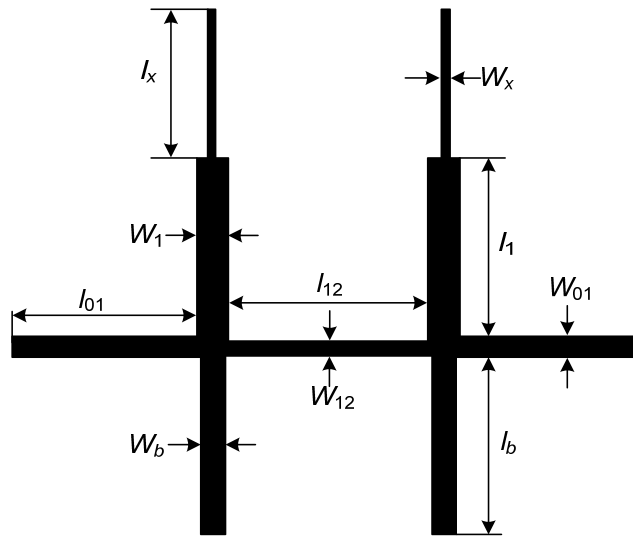
(a)
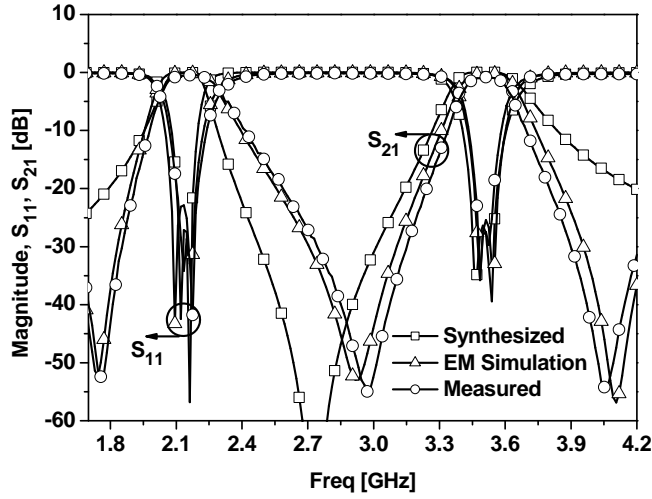
(b)

Fig. 2.10. Proposed microstrip dual-band Filter III : (a) physical layout and (b) simulation and measurement results.

2.3.2 Dual-band Filter With Different Fractional Bandwidths

The Filter IV specification is the same as for Filter II in the previous section. The calculated values of elements shown in Fig. 2.6(b) for n=2 are $J_{01}=J_{23}=0.0172$, $J_{12}=0.0155$, $J_{x1}=J_{x2}=0.032$, $L_{b1}=L_{b2}=3.2970$ nH, $C_{b1}=C_{b2}=0.3476$ pF, $L_{x1}=L_{x2}=3.4393$ nH, and $C_{x1}=C_{x2}=0.4919$ pF, respectively.

The physical layout of Filter IV is shown in Fig. 2.11(a) and the dimensions are $W_{01}=2.178$, $l_{01}=11.90$, $W_{12}=1.60$, $l_{12}=11.96$, $W_x=0.4$, $l_x=12$, $W_1=2.2$, $l_1=12.10$, $W_b=0.596$, and $l_b=11.86$ mm, respectively. Fig. 2.11(b) shows the simulation and measurement results.
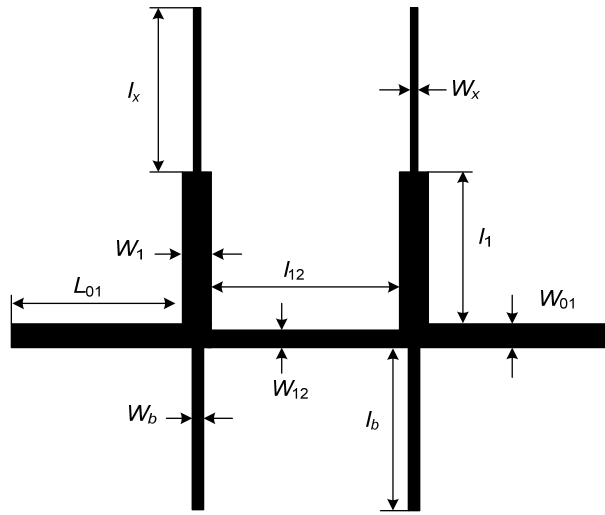
(a)
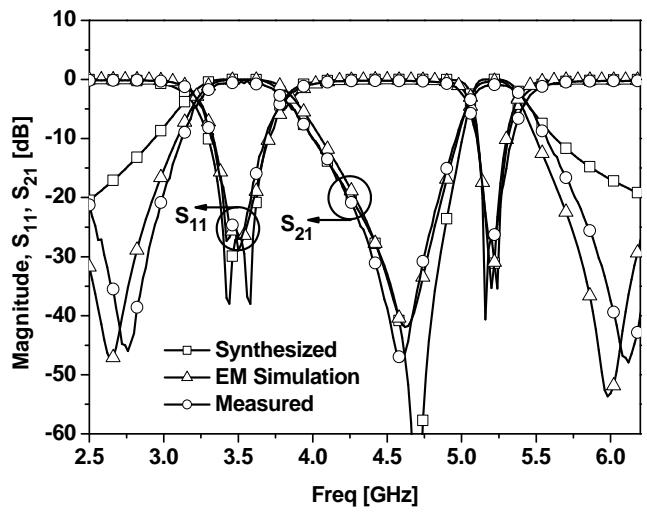
(b)

Fig. 2.11. Proposed microstrip dual-band Filter IV : (a) physical layout and (b) simulation & measurement results.

The measured insertion losses in the passbands are 0.95 dB and 1.1 dB at 3.5 GHz and 5.2 GHz, respectively. The return loss at 3.4-3.6 GHz and 5.15-5.25 GHz are greater than 19 dB. The measured bandwidths are 190.6 MHz and 101.2 MHz, for which the FBWs are 5.44 % and 1.94 %, respectively.

2.4 Summary and Discussion

We demonstrated the design method for dual-band BPF with the arbitrary bandwidths. We use the novel frequency mapping function in this chapter. Simple analytical design equations are presented and the circuit elements of the proposed dual-band bandpass filters are calculated from the low-pass filter by applying a simple frequency mapping function. In order to implement the dual-band BPF for the microwave frequency, circuit conversion techniques have been applied for easy realization with distributed transmission lines.

In order to validate the proposed method, two type filters having the same and different fractional bandwidths are presented with LTCC as well as microstrip-line technology. The simulation and measurements results are in good agreement with the theoretical design results. The proposed method should be flexible enough to enable the design of bandpass filters with two passbands of significantly different bandwidths.

CHAPTER 3

DESIGN OF DUAL-BAND BANDPASS FILTER USING DGS WITH TUNABLE SECOND PASSBAND

In this chapter, a variable characteristic impedance transmission line that can be used to the design of dual-band BPF, is presented. The proposed dual-band filter offers the fixed first passband and the tunable second passband. The tuning of the second passband is achieved by varying the characteristic impedance of open shunt stub line in a SLR with the help of the DGS transmission line and varactor diodes. In order to validate the proposed structure, a two stage dual-band BPF with three transmission zeros was implemented and experimentally verified based on its theoretical predictions and simulations.

3.1   The Stub Loaded Resonator Characteristics

Fig. 3.1 shows the proposed structure of the tunable SLR, which consists of series resonators and an open shunt stub at the junction point between the series resonators. Assuming Y_1, θ_1 and Y_2, θ_2 as the characteristic admittance and electrical length of the series resonators and the open shunt stub, respectively, the input admittance of the proposed structure is given by :

$$Y_{\text{in}} = jY_1 \frac{2Y_1 \tan\theta_1 + Y_2 \tan\theta_2}{Y_1 - \left(Y_1 \tan\theta_1 + Y_2 \tan\theta_2\right)\tan\theta_1} \tag{3.1}$$

The resonant condition can be obtained by setting Y_{in}=0, which is obtained as :

$$2Y_1 \tan\left(a\theta_1\right) + Y_2 \tan\left(a\theta_2\right) = 0 \tag{3.2}$$

Where a is the ratio of the higher mode resonant frequency (f_r) to the fundamental resonant frequency (f_1). The fundamental resonance can be obtained from (3.2) by setting $a=1$ and $\theta_1=90^o$.
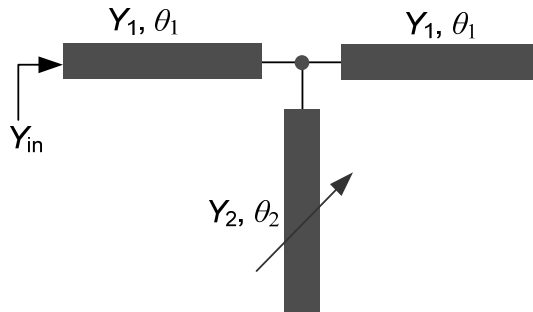
Fig. 3.1. Structure of tunable stub loaded resonator.

The relationship between the first two resonant frequency ratios (f_r/f_1) and the impedance ratio ($K=Z_2/Z_1$) of the SLR is plotted in Fig. 3.2 using MATLAB.
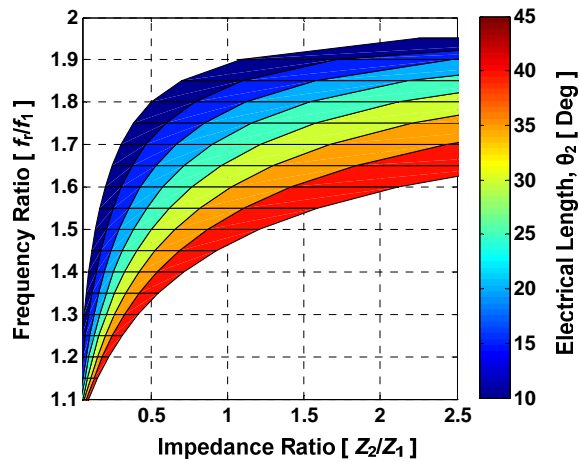
Fig. 3.2. Dependence of resonant frequency ratio according to characteristic impedance of open stub.

Color bar represents electrical length of open stub.

36

From this figure, it is clear that by keeping the electrical length of the open shunt stub fixed, the frequency ratio (f_r/f_1) can be tuned by varying the impedance ratio (Z_2/Z_1) of the SLR. This SLR characteristic is applied in the design of the dual-band BPF with the tunable second passband.

3.2   The Variable Characteristic Impedance Transmission Line

Transmission lines with modified ground structure, such as a photonic band gap and a DGS, have been actively studied and applied successfully in the design of various microwave circuits [52]-[53]. The key idea of this work is to apply the variable characteristic impedance transmission line to the design of dual-band BPF. Fig. 3.3 shows the structure of the variable characteristic impedance transmission line which consists of a conventional microstrip signal line, the DGS ground island and varactor diodes located in the bottom plane of the microstrip line. The varactor diodes are mounted between the DGS ground island and the ground plane.
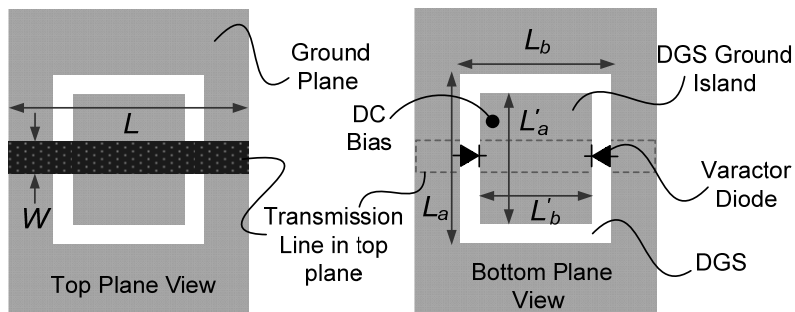
Fig. 3.3. Variable characteristic impedance transmission line with DGS ground island and varactor diodes.

The characteristic impedance of the modified microstrip line can be tuned as

the result of change in the capacitance of the ground plane of the microstrip line with the help of the varactor diodes. The physical dimensions of the variable impedance transmission line are shown in Table 3.1, where the used substrate is RT/Duroid-5880 of Rogers Corporation with a dielectric constant (ε_r) of 2.2 and thickness (h) of 31 mils. The characteristic impedance of the transmission line with the modified ground structure can be calculated by applying reflection and transmission theories [54]. Using the method described in [54], the proposed structure has been simulated with HFSS v11 of Ansoft and the calculated characteristic impedances are plotted in Fig. 3.4. The characteristic impedances of this modified line can be varied over 47.5-86 Ω by changing the capacitance between 20-1.5 pF at 1.4 GHz.

To verify the application of variable characteristic impedance line in tunable SLR, the full wave EM simulation was performed and resonant characteristics of tunable SLR are plotted in Fig. 3.5. The two transmission lines with 50 Ω characteristic impedance are utilized to feed proposed SLR using a loose coupling. The dimension of DGS is same as given in Table 3.1.

TABLE 3.1. DIMENSIONS OF VARIABLE CHARACTERISTIC IMPEDANCE TRANSMISSION LINE WITH DGS AND VARACTOR DIODES (DIMENSIONS ARE IN MILLIMETERS), REFER TO FIG. 3.3 FOR NOTATION.

W	L	L_a	L_b	L'_a	L'_b
2.5	11.5	6	9.9	6.3	8.1
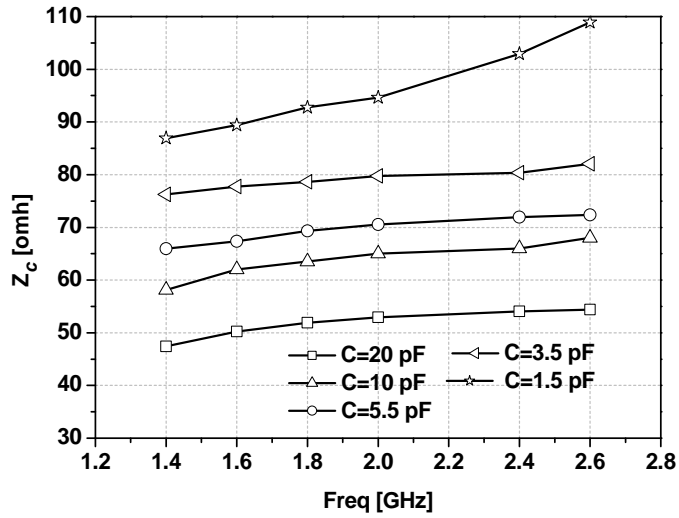
Fig. 3.4. Calculated characteristic impedances of the proposed variable impedance microstrip line.

As seen from the Fig. 3.5, the second resonant frequency can be tuned with the help of DGS and varctor diodes in the ground plane, whereas the first resonant frequency is preserved.
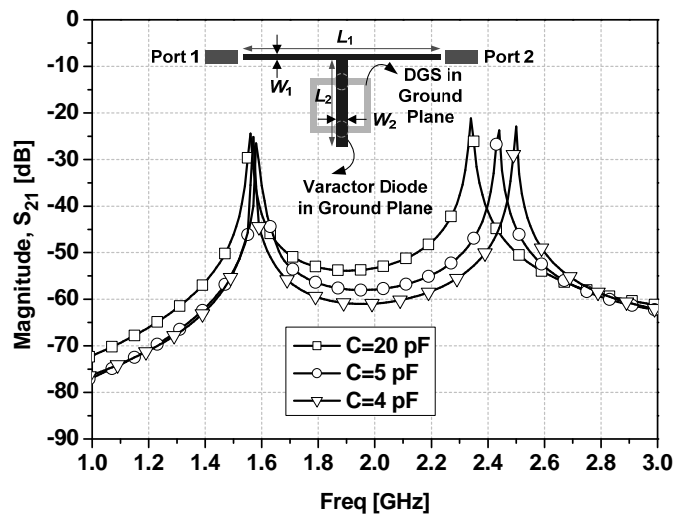
Fig. 3.5. Resonance frequency of tunable SLR according to capacitance (L_1=72.5, L_2=10.8, W_1=0.65 and W_2=2.5 [mm]).

3.2   The Simulation and Experimental Results

Fig. 3.6 shows the structure of the proposed dual-band BPF, which consists of SLRs in the signal plane, the DGS ground island and varactor diodes in the ground plane. The microstrip lines are folded in order to reduce the size, forming open loops. The goal was to design the BPF with the first passband center frequency of 1.575 GHz and tunable the second passband center frequency around 2.40 GHz. The electrical lengths of θ_1 and θ_2 were calculated as 90° and 30° at 1.575 GHz, respectively. The initial characteristic impedances of the SLRs were determined as Z_1=100 Ω and Z_2= 48 Ω.

The physical dimensions of the proposed filter V are shown in Table 3.2. The used varactor diodes were SMV 1234-011LF of Skyworks, whose capacitances range over 1.2-30 pF according to the bias range of 15-0 V. However, the varactor diode is considered as ideal variable capacitance in simulation for the convenient.
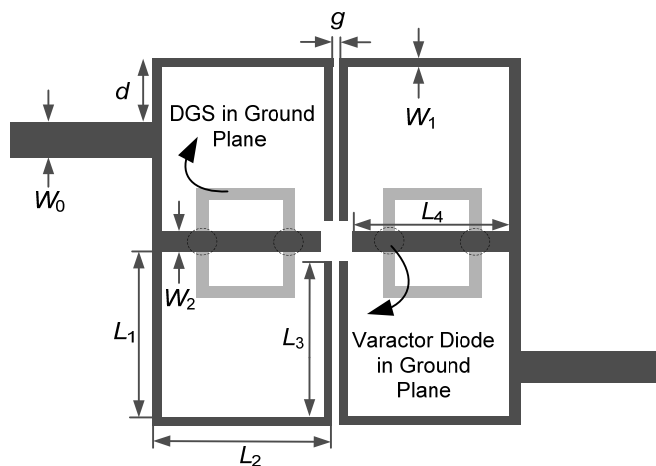
Fig. 3.6. Proposed dual-band bandpass filter V in top view .

TABLE 3.2. DIMENSIONS OF FIG 3.6 (DIMENSIONS ARE IN MILIMETERS).

$W_0/W_1/W_2$	$L_1/L_2/L_3/L_4$	d/g
2.38/0.65/2.5	10.5/13.3/11.2/10.8	3.95/0.5

The simulated and measured results according to the varactor diode bias voltage are plotted in Fig. 3.7. A close agreement between them can be observed. As described in the previous section, the performance of the first passband remains almost constant. Possessing the central frequency of 1.575 GHz, the first passband has a 3-dB fractional bandwidth of 16.8 % and the maximum insertion loss of 0.59 dB.
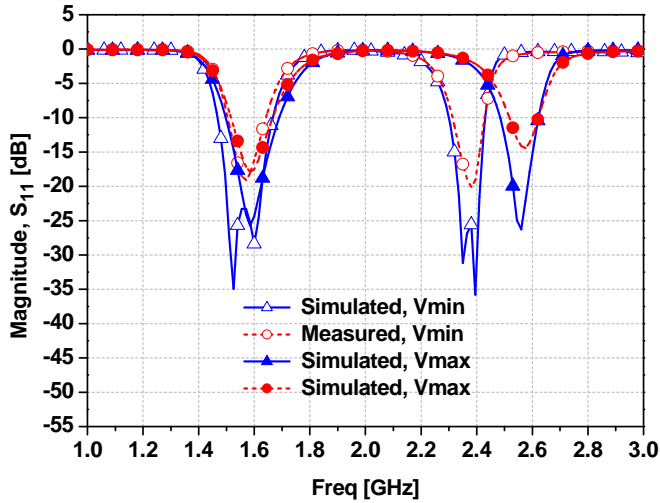
(a)
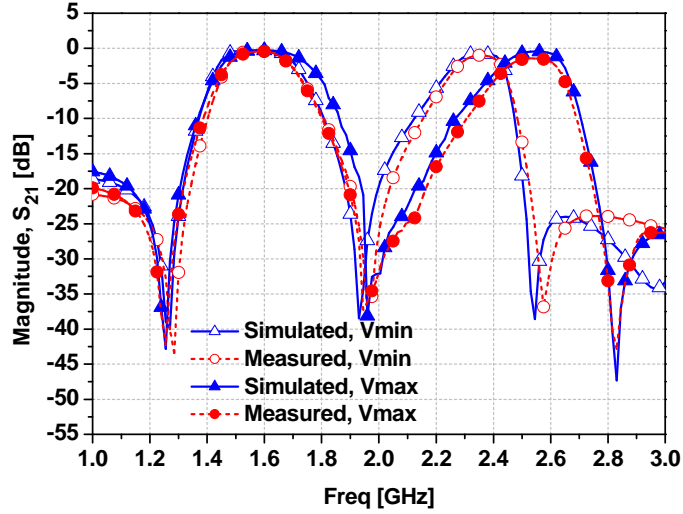
(b)

Fig. 3.7. Simulated and measured results of (a) return loss response and (b) insertion loss response according to varactor diode bias voltage (V_{min}=0 V, V_{max}=8.2 V).

The maximum return loss is larger than 18.9 dB at the center frequency. In addition, the second passband center frequency is tunable between 2.38 and 2.56 GHz (f_r/f_1=1.51~1.62 as f_1=1.575 GHz) by varying the varactor diode bias voltage over 0-8.2 V, as shown in Fig. 3.7. The measured insertion loss varies from 1.112 to 1.438 dB with an almost constant fractional bandwidth of 7.5 %. The maximum return loss is larger than 14.1 dB at center frequency of the second passband throughout the entire controllable range.

The proposed filter creates three transmission zeros for each bias-voltage. The two transmission zeros generated by two transmission line arms (from tapping position to two ends of the open loop as shown in Fig. 3.6) that correspond to 90° at the frequencies of two transmission zeros around both sides of first passband, are

fixed. The remaining transmission zero located on the higher side of the second passband generated as the input impedance viewed from tapping position toward the loaded stub approaches zeros at frequency of transmission zero, which moves synchronously with the tuning of the second passband due to change in propagation constant of stub with the help of DGS and varactor diodes in the ground plane. These characteristics of the proposed filter improve the selectivity of the out band frequencies. The photograph of fabricated filter is shown in Fig. 3.8.
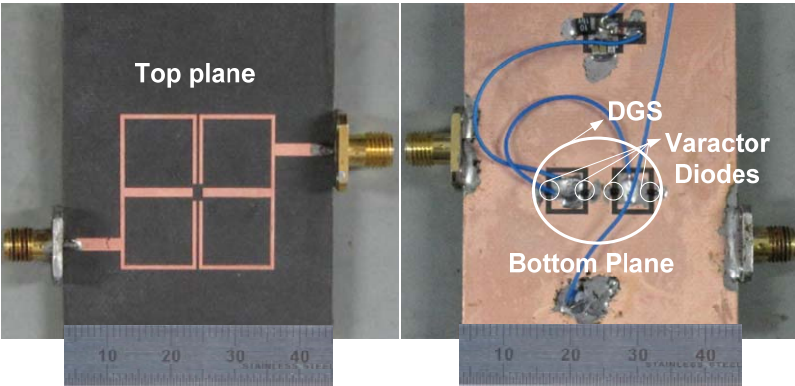
Fig. 3.8. Photograph of fabricated filter V.

3.3 Summary and Discussion

The novel design of dual-band bandpass filter with the tunable second passband using a variable characteristic impedance of the stub in the SLR is presented in this chapter. The characteristic impedance of the stub can be controlled with the help of the defected ground structure and the varactor diodes located in the ground plane. Both theoretical analysis and experiments were done in order to validate the

proposed structure. It was demonstrated that the second passband can be adjusted while keeping the first passband fixed. The proposed filter provides low insertion losses throughout the entire tuning range of the second passband which is expected to be applicable to global positioning systems (GPS) and wireless local area networks (WLANs).

CHAPTER 4

HARMONIC SUPPRESSED DUAL-BAND BANDPASS FILTERS WITH TUNABLE PASSBANDS

With tunable passband frequency characteristic in tunable filters, the harmonic bands which degrade the out-of passband characteristics, are also tuned. Thus, the suppression of harmonics is one of critical issues for tunable filters. This issue has rarely been addressed in the design of tunable dual-band filters.

In this chapter, a novel approach to the design of tunable dual-band BPFs with broadband harmonic suppression characteristics is presented. The proposed filter offers the possibility of two tunable passbands as well as a fixed first passband and tunable second passbands.

4.1 Characteristics of Proposed Resonator

Fig. 4.1 (a) shows the basic structure of the proposed resonator. It consists of a transmission line and three varactor diodes. For the theoretical analysis, it is assumed to be a lossless transmission line of characteristic admittance Y and physical length L. Two varactor diodes are attached at the ends of the transmission line and one varactor diode is placed at a center point of the transmission line. For simplicity, the parasitic elements of varactor diodes are ignored. Since the structure is symmetrical, the even- and odd-mode analysis method is applicable to obtain the resonant frequencies [50].

4.1.1 Odd-mode Excitation Analysis

When the odd-mode excitation is applied to the ends of the proposed resonator shown in Fig. 4.1(a), there is a voltage null along the symmetry plane.

(a)

(b)

(c)
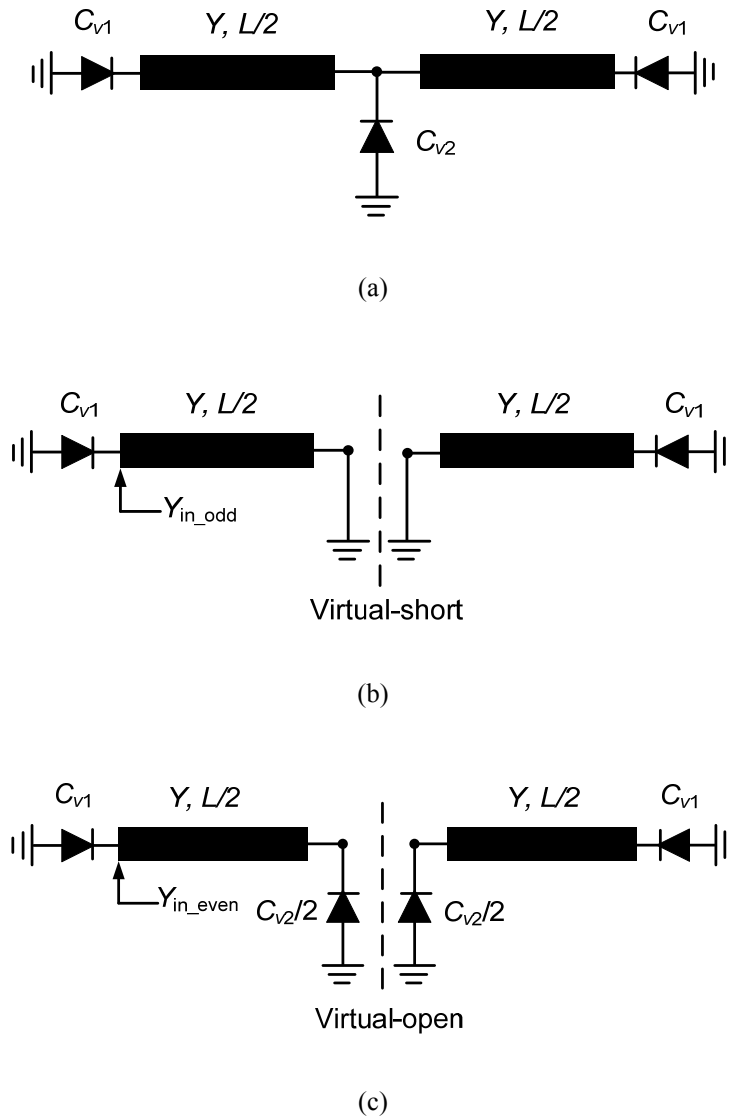
Fig. 4.1. (a) Basic structure of the proposed resonator, (b) odd-mode excitation equivalent circuit, and (c) even-mode excitation equivalent circuit.

Under the odd-mode excitation, it can be represented by the half circuit as given in Fig. 4.1(b). The odd-mode input admittance is given as follows.

$$Y_{\text{in\_odd}} = j\left[\omega_{odd}C_{v1} - Y\cot\left(\beta L/2\right)\right]$$ (4.1)

Where C_{v1} is the capacitance of the varactor diode connected at the end of the line and β is the propagation constant of the transmission line. From the resonance condition of $\text{Im}(Y_{\text{in-odd}})=0$, the odd-mode resonant frequency can be determined as follows.

$$f_{odd} \times \tan\left(\frac{\pi f_{odd}L}{v_p}\right) = \frac{Y}{2\pi C_{v1}}$$ (4.2)

Where v_p is the phase velocity. The fundamental odd-mode resonant frequency can be used as the passband frequency. From (4.2), it is concluded that the odd-mode resonant frequency fully depends on the capacitance C_{v1} of varactor diode connected at the ends of the transmission line. Therefore, the change of the bias voltage on both end varactor diodes will result in the change of passband frequencies, enabling the tunability of the first passband frequency. Moreover, the odd-mode resonant frequencies are not affected by the varactor diode connected at the center of the transmission line.

4.1.2 Even-mode Excitation Analysis

For the even-mode excitation, there is no current flowing through the center of the transmission line. Under the even-mode condition, the proposed resonator can

be represented by the equivalent half circuit shown in Fig. 4.1(c). The even-mode input admittance is given as follows.

$$Y_{in\_even} = j\left(\omega_{even} C_{v1} + Y \frac{\omega C_{v2}/2 + Y\tan\left(\beta L/2\right)}{Y - \omega\tan\left(\beta L/2\right)C_{v2}/2} \right) \tag{4.3}$$

Where C_{v2} is the capacitance of the varactor diode connected at the center of the transmission line. For the resonance condition, the even-mode resonant frequency can be determined as.

$$\left(f_{even} - \frac{Y^2}{2\pi^2 f_{even} C_{v1} C_{v2}} \right)\tan\left(\frac{\pi f_{even} L}{v_p} \right) = \frac{Y\left(C_{v1} + C_{v2}/2\right)}{\pi C_{v1} C_{v2}} \tag{4.4}$$

The fundamental even-mode resonant frequency can be utilized as the passband frequency. From (4.4), it is observed that the even-mode resonant frequency depends on C_{v1} and C_{v2}. Thus, the change of the bias voltages applied to all of the varactor diodes will also result in the change of passband frequency, enabling the tunability of the second passband frequency. Moreover, when C_{v1} is fixed, the even-mode resonant frequency can be tuned with the help of C_{v2} alone. This characteristic of the proposed resonator can be used to design a dual-band BPF with the tunable second passband (even-mode resonant frequency) and the fixed first passband (odd-mode resonant frequency).

To verify the above theoretical analysis, a full-wave electromagnetic (EM) simulation was carried out by using HFSS v11 of Ansoft and resonant frequency characteristics of proposed resonator is plotted in Fig 4.2. Two microstrip lines

with a characteristic impedance of 50 Ω are utilized to feed the proposed resonator using a loose coupling to investigate its resonant behavior. The length of resonator is fixed at 40 mm.

Fig. 4.2(a) shows the simulated magnitude of S_{21} according to different capacitances of varactor diodes. As capacitances are varied, the odd- and even-mode resonant frequencies are tuned simultaneously. This characteristic of the proposed resonator can be utilized to the design of dual-band BPF with two tunable passbands.

Fig. 4.2(b) shows the simulated magnitude of S_{21} in case where the capacitance of the varactor diodes connected at the end of the transmission line are fixed. Under this condition, it is obvious when the odd-mode resonant frequency is fixed, then the even-mode resonant frequency can be tuned by only varying the capacitance of the varactor diode connected at the center of the transmission line.
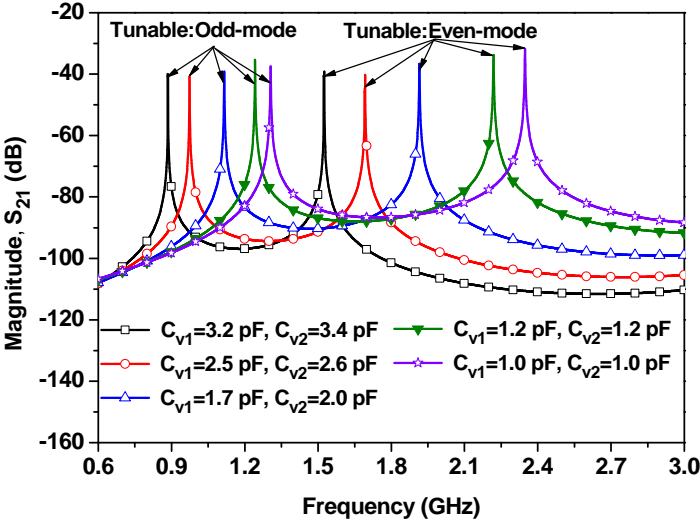
(a)
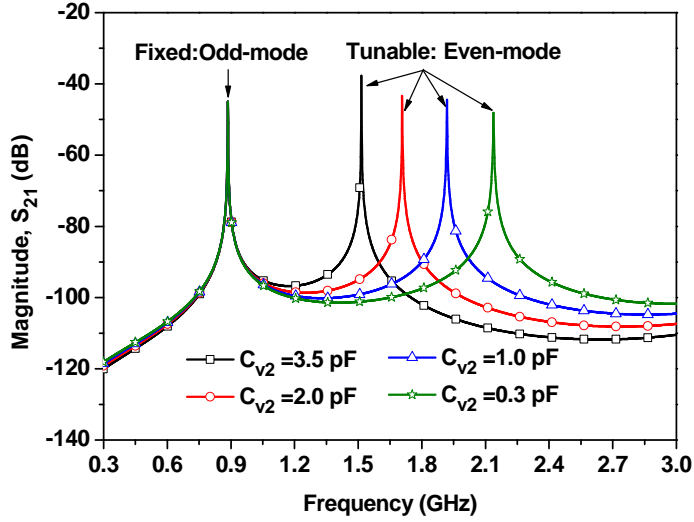
(b)

Fig. 4.2. Resonant frequencies according to capacitances : (a) tunable odd and even mode and (b) fixed odd mode and tunable even-mode frequencies with fixed C_{v1}=3.2 pF.

By varying the value of C_{v2} from 3.5 to 0.3 pF, the even-mode resonant frequency can be varied from 1.5 to 2.3 GHz. This characteristic of proposed resonator can be utilized to design a dual-band BPF with the fixed first passband and tunable second passband.

4.2. External Quality Factor (Q_e)

In order to find the external quality factor, the configuration of the tapped resonator is shown in Fig. 4.3. To facilitate the analysis, the effects of line discontinuity are ignored. The input admittance (Y_L) of the resonator seen from the center of the line is given as follows.

$$Y_L = j \left[\omega C_{v2} + Y \frac{\omega C_{v1} + Y \tan\left(\dfrac{\omega L}{v_p}\right)}{Y - \omega C_{v1} \tan\left(\dfrac{\omega L}{v_p}\right)} \right] \tag{4.5}$$

The overall input admittance (Y_{in}) of resonator seen from the input port is given as follows.

$$Y_{in} = j \left[\frac{\omega C_{v1} + Y \tan\left(\dfrac{\omega L_1}{v_p}\right)}{Y - \omega C_{v1} \tan\left(\dfrac{\omega L_1}{v_p}\right)} \right] + Y \frac{Y_L + jY \tan\left(\dfrac{\omega L_2}{v_p}\right)}{Y + jY_L \tan\left(\dfrac{\omega L_2}{v_p}\right)} \tag{4.6}$$

The external quality factor (Q_e) is then determined as follows.

$$Q_e = \frac{\omega_0}{2Y_0} \left. \frac{\partial \, \mathrm{Im}\left[Y_{in}\right]}{\partial \omega} \right|_{\omega = \omega_0} \tag{4.7}$$

It can be seen that the lengths of the transmission line L_1 and L_2 will affect on Q_e. By properly choosing these parameters, the desired Q_e can be obtained within the frequency tuning range.
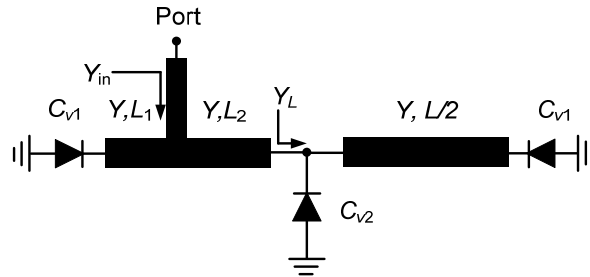
Fig. 4.3. Resonator with input coupling network.

4.3. Coupling Coefficient (K_i)

Fig. 4.4 shows the arrangement of resonators for EM simulation to analyze the coupling coefficient between resonators according to two parameters, g_1 and L_3, which are gap between the resonators and coupling length of two resonators, respectively. The other parameters used in the simulation are shown in Fig. 4.4. To decrease the effect of input-output on the coupling coefficient between resonators, a weak input-output feed is used. In this simulation, the ideal capacitors were used. The coupling characteristic between resonators are simulated and drawn with respect to g_1 in Fig. 4.5. As seen from Fig. 4.5, the separation of resonant frequencies can be controlled with g_1.
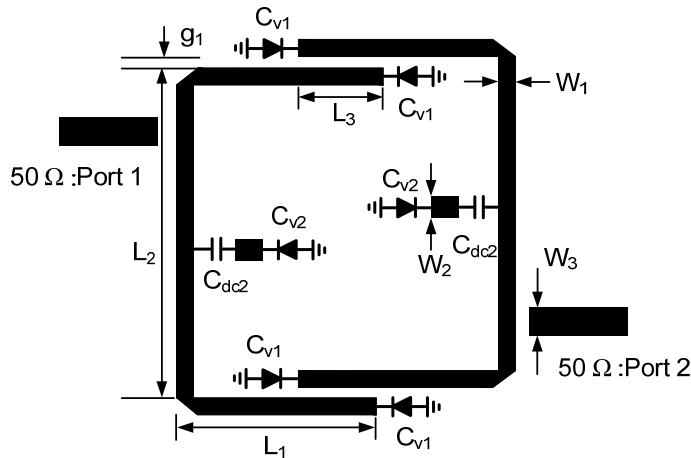
Fig. 4.4. Layout for examining the coupling between resonators.

TABLE 4.1. DIMENSIONS OF FIG. 4.4 (DIMENSIONS ARE IN MILIMETERS).

$W_1/W_2/W_3$	$L_1/L_2/L_3$	C_{dc2} [pF]
1.8/1.8/2.4	17.2/34.28/10	3.90
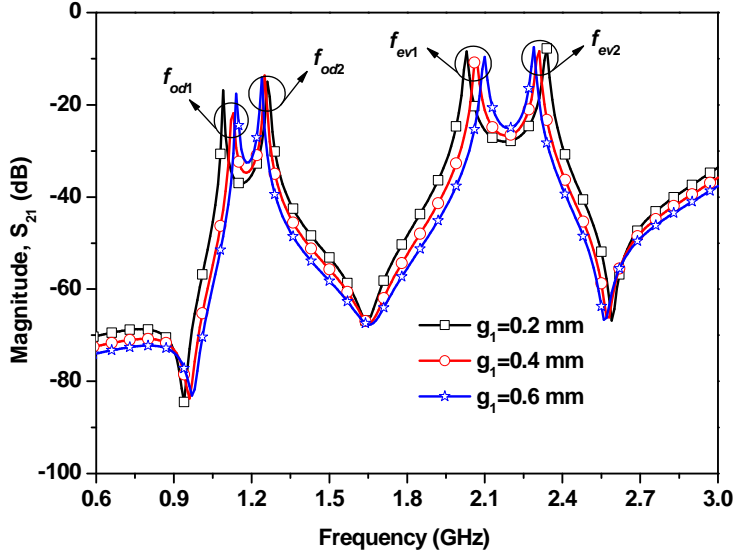
Fig. 4.5. Coupling characteristic between resonators with respect to g_1 in case of L_3=10 mm, C_{v1}=1 pF, and C_{v2}=0.9 pF.

For the sake of estimating and designing the two passbands, the coupling coefficient of each bands can be calculated by the following common formulas.

$$K_1 \approx \frac{f_{od2}^2 - f_{od1}^2}{f_{od2}^2 + f_{od1}^2} \quad K_2 \approx \frac{f_{ev2}^2 - f_{ev1}^2}{f_{ev2}^2 + f_{ev1}^2} \tag{4.8a}$$

$$\frac{K_1}{K_2} \approx \frac{\Delta_1}{\Delta_2} \tag{4.8b}$$

Where K_1 and K_2, f_{odi}, f_{evi} (i=1, 2), Δ_1 and Δ_2 are coupling coefficients, odd and even-mode resonant frequencies and FBWs at the first and second passbands, respectively.
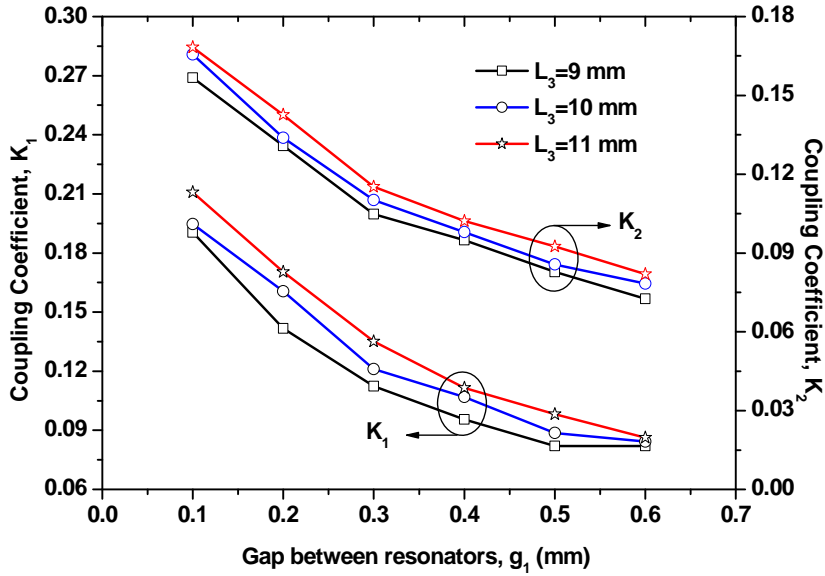
Fig. 4.6. Calculated coupling coefficient with respect to g_1 and L_3 in case of $C_{v1}=1$ pF and $C_{v2}=0.9$ pF.

With combined adjustments of f_{od1}, f_{od2}, f_{ev1} and f_{ev2}, the first and second passbands are established and determined. Therefore, the bandwidth of the two passbands can be controlled by changing their coupling coefficients. For design graph chart, the coupling behaviors between resonators are simulated and the estimated coupling coefficients are drawn in Fig. 4.6 as a function of g_1 and L_3.

4.4. Filter Implementation and Verification

To verify the analytical analysis of the proposed resonators, two types of tunable dual-band BPF were designed, simulated and measured. The used substrate is an RT/Duriod 5880 made by Rogers with a dielectric constant (ε_r) of 2.2 and thickness (h) of 31 mils.

4.4.1 Tunable Dual-band Bandpass Filter without Harmonic Suppression

Fig. 4.7 depicts the configuration of the second order microstrip tunable dual-band filter VI. In the proposed filter, four varactors are attached at the ends of the two microstrip lines and two varactor diodes are attached at the center of the two microstrip lines. The resonators are folded in order to reduce the size, forming open loops.

The varactor diodes are SMV1233-079LF from Skyworks Solutions Inc. The input/output lines are tapped at the resonators. Two capacitors (C_{dc1}) are attached in the feeding lines, functioning as a dc block. Another two dc block capacitors (C_{dc2}) are attached at the center of line.

Fig. 4.7. Configuration of filter VI with physical dimensions and varactor diode equivalent circuit model with C_p=0.51 pF, R_s=1.2 Ω, L_s=0.7 nH.

TABLE 4.2. DIMENSIONS OF FIG. 4.7 (DIMENSIONS ARE IN MILIMETERS).

$W_1/W_2/W_3$	$L_1/L_2/L_3/L_4$	g_1	C_{dc1}/C_{dc2} [pF]
1.2/0.4/2.4	17.2/27.6/5.3/10	0.4	20/3.90

The simulation was accomplished by using Advanced Design System (ADS) 2011 of Agilent Technologies. In this simulation, the SPICE model of varactor diode provided by the manufacturer was used as shown in Fig. 4.7. The measured capacitance and series resistance (R_s) of varactor diode is shown in Fig. 4.8. After the simulation, the physical parameters and component values of the filter are determined as shown in Table 4.2.

Fig. 4.9 shows the simulation and measurement results of filter VI for the several typical bias voltages. The measurement results agree well with the simulation results. The measurement results show that the first passband frequency can be tuned from 0.85 to 1.2 GHz with almost constant 3-dB FBW of 13 % and the second passband frequency can be tuned from 1.40 to 2.14 GHz with an 3-dB FBW of 11%.

Fig. 4.8. Measured capacitance and series resistance (R_s) of the varactor diode SMV 1233-079LF.

(a)

(b)

Fig. 4.9. Simulation and measurement results of filter VI with tunable both passbands: (a) return loss and (b) insertion loss. Reverse bias voltage variation : V_{Cv1}=1.5~15 V and V_{Cv2}=0.4~15 V.

The return loss is better than 12 dB in the overall tuning range of both passbands as shown in Fig. 4.9(a).The insertion loss varies from 0.85 to 2.42 dB at the first passband, whereas it varied 1.20 to 3.30 dB at the second passbands as shown in Fig. 4.9(b). As the passbands are tuned towards lower frequencies, the insertion loss becomes higher because the microstrip line becomes electrically shorter as a result decreasing the overall resonator Q value.

For each bias voltage, the proposed filter provides three transmission zeros near the passbands in order to improve the selectivity of the filter. The two transmission zeros generated by two transmission line arms (from tapping position to two ends of open loop as shown in Fig. 4.7) corresponds to an electrical length of 90° at the frequencies of transmission zeros. The remaining transmission zero located on the higher side of the second passband is generated as the input impedance viewed from tapping position toward center loaded varactor diode, approaches zeros at frequency of transmission zero. These transmission zeros move along the passbands.

Fig. 4.10 shows the simulation and measurement results of filter VI with the fixed first passband and tunable second passband frequency. As seen from this figure, the first passband frequency is constant at 1.070 GHz with 3-dB FBWs of 13% by keeping the bias voltage of varactor diodes connected at the line ends fixed. The second passband is tuned with the bias voltage of varactor diode loaded at the center of the line. From the measurement result, it is found that the second passband frequency can be tuned from 1.70 to 1.98 GHz with almost constant 3-dB FBWs of 11%. The return loss is better than 15 dB for entire tuning range of the

second passband, as shown in Fig. 4.10(a). The insertion loss varies from 1.15 to 2.76 dB as shown in Fig. 4.10(b). Fig. 4.11 shows a photograph of the fabricated filter VI.

(a)
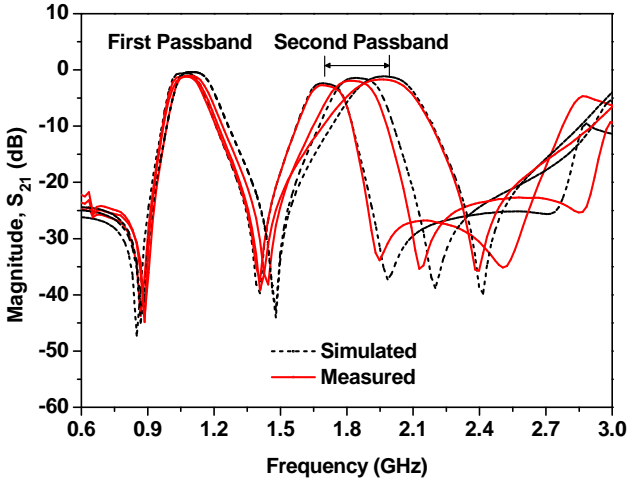
(b)

Fig. 4.10. Simulation and measurement results of filter VI with fixed first passband and tunable second passband: (a) return loss and (b) insertion loss characteristics. Reverse bias voltage variation: V_{Cv1}=5.45 V and V_{Cv2}=3.08~15.
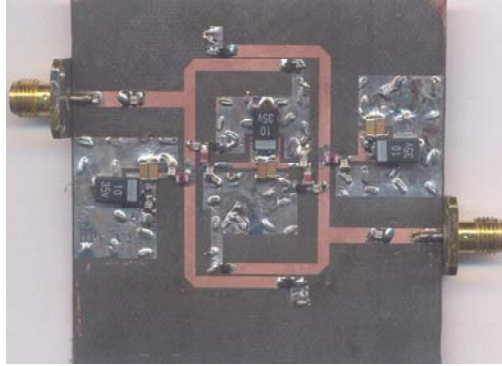
Fig. 4.11. Photograph of fabricated filter VI.

4.4.2 Tunable Dual-band Bandpass Filter with Harmonic Suppression

From the simulation and measurement results described in the previous section, it is found that there are several harmonics of the two passbands and these harmonics are also tuned by varying the passband frequencies. These unwanted harmonics generated by filter must be suppressed. A simple method of suppressing the harmonic is to introduce a transmission zero at the harmonic frequency [55]. However, this method will be inefficient, because it can only suppress the harmonics around a specific frequency. In the case of the tunable dual-band BPF, the harmonic frequency variation range is too broad which are not sufficient to reject harmonics by the simple transmission zero circuit.

The DGS of microstrip line is implemented by making artificial defects on the ground plane and provides band-rejection characteristics at a certain resonance frequency band corresponding to the size of defect and its shape on the ground plane. The DGS also provides an additional effective inductance of the transmission line, which enables the slow-wave factor of line to be increased.

These band-rejection properties and slow-wave effect of the DGS have been applied in the design of various microwave circuits such as filters, dividers, and amplifier [52]-[53], [56]-[58]. In microwave circuits, the band-rejection property of the DGS can also be utilized in the suppression of harmonics [59]-[61].

Fig. 4.12 shows the proposed configuration of the harmonic suppressed tunable dual-band filter VII. In this structure, the DGS is used at the input/output feeding lines for inducting coupling and acts as the broad band-rejection resonator to suppress the harmonics of filter VI. The methods for finding the equivalent circuits of DGS are detailed in [52]. The EM simulation was performed using HFSS v11 of Ansoft with considering ideal capacitors. After simulation, the physical parameters and component values of the filter are determined as shown in Table 4.3.
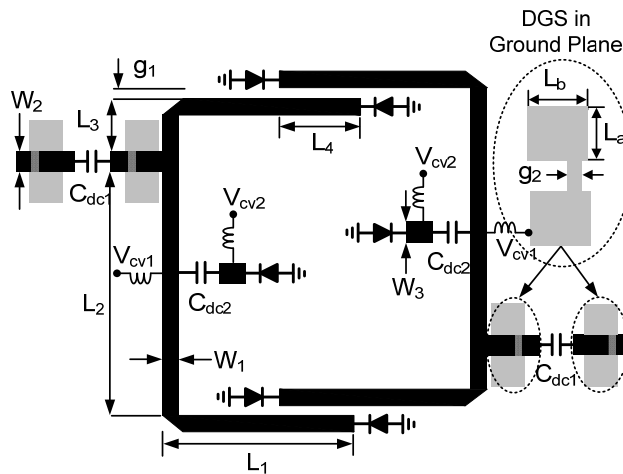
Fig. 4.12. Configuration of filter VII and physical dimensions.

TABLE 4.3. DIMENSIONS OF FIG. 4.12 (DIMENSIONS ARE IN MILIMETERS).

$W_1/W_2/W_3$	L1/L2/L3/L4/L_a/L_b	g_1/g_2	C_{dc1}/C_{dc2} [pF]
1.2/0.4/2.4	17.2/27.6/5.3/10/6/6	0.64/0.4	20/3.90

Fig. 4.13 shows the simulation and measurement results of filter VII. The passband frequencies are tuned with the help of the bias voltages of the varactor diodes. From the measurement results, the first passband frequency can be tuned from 0.85 to 1.2 GHz with 3-dB FBW of 13 % and the second passband frequency can be tuned from 1.45 to 2.08 GHz with 3-dB FBW of 11 %. The return loss i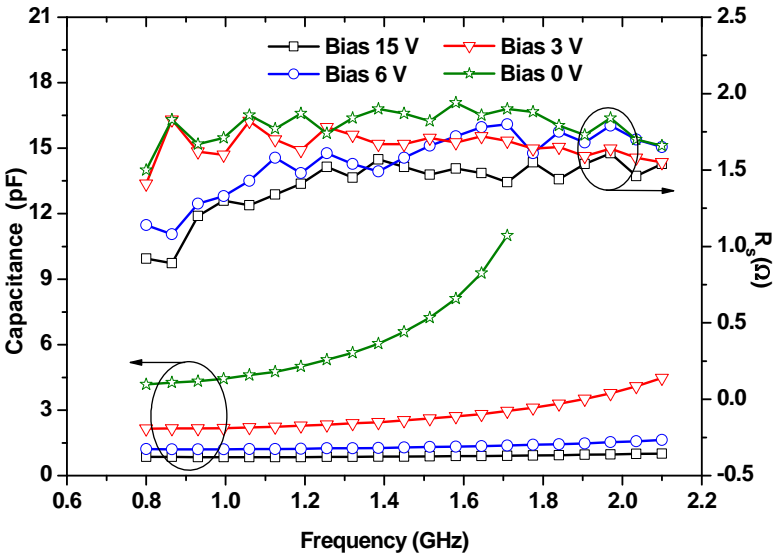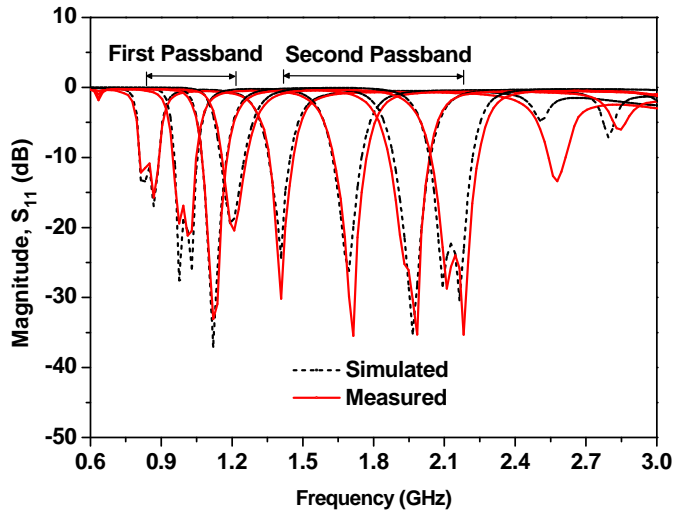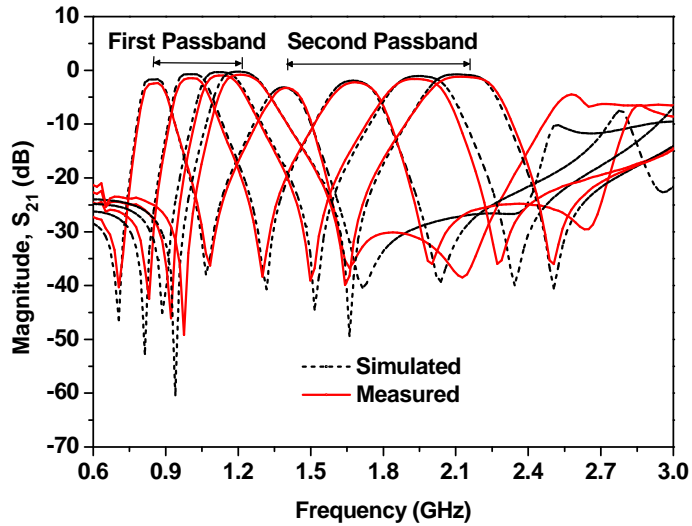s better than 13 dB over the entire tuning range of the passbands as shown in Fig. 4.13(a). The insertion loss varies from 1.32 to 3.4 dB at the first passband and 1.8 to 3.80 dB at the second passband as shown in Fig. 4.13(b).

The insertion loss differences between the simulation and measurement results are due to the use of ideal capacitances in EM simulation. These measurement results for filter VII are almost similar with filter VI results provided in the previous section except for the suppression of the harmonic characteristics
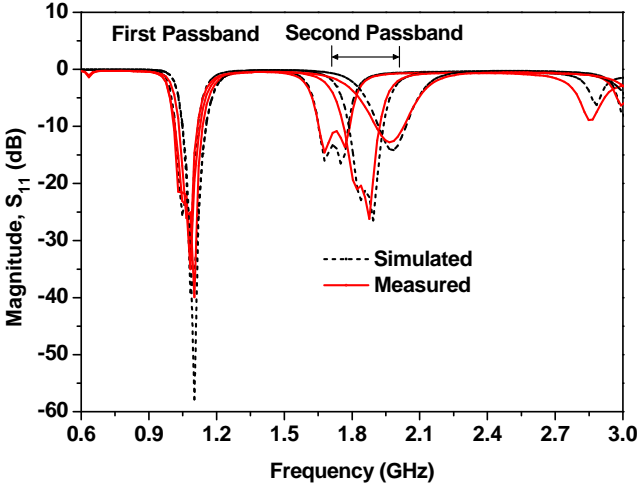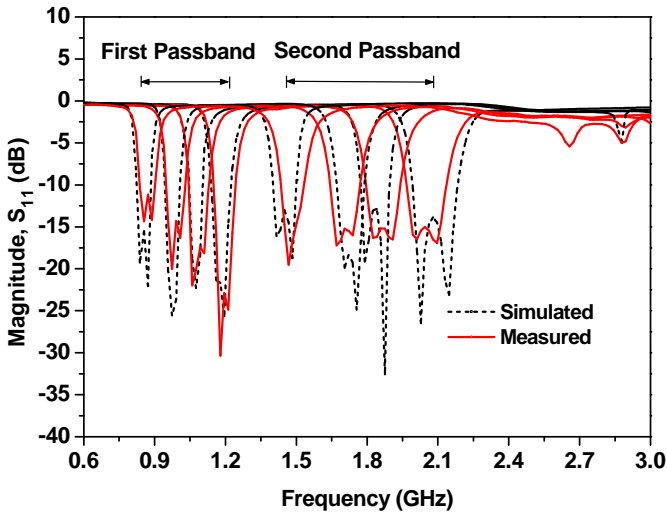

(a)
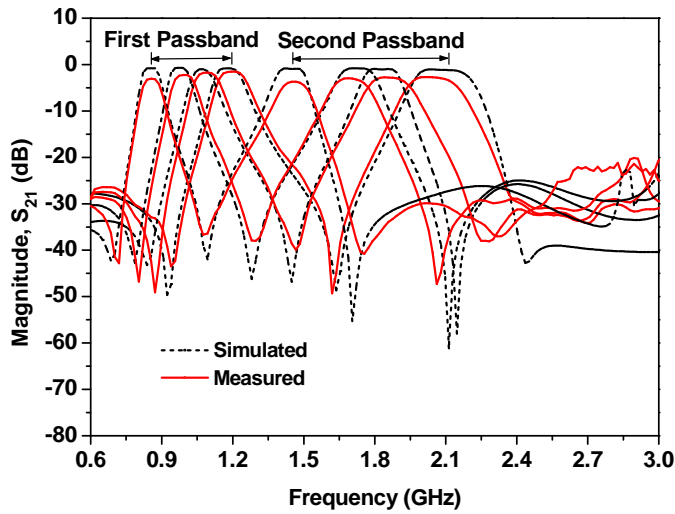
(b)

Fig. 4.13. Simulation and measurement results of filter VII with tunable both passbands : (a) return loss and (b) insertion loss characteristics. Reverse bias voltage variation : V_{Cv1}=1.8~15 V and V_{Cv2}=1~15 V.

Fig. 4.14 shows the simulation and measurement results of filter VII with the fixed first passband and tunable second passband frequency. The first passband frequency is held constant at 1.070 GHz by fixing the bias voltage of varactor diodes connected to the ends of the line. The second passband frequency is tuned from 1.75 to 1.97 GHz. The return loss variation is better than 15 dB throughout of tuning range of the passbands. Similarly, the variation of the insertion loss is 1.87 to 3.2 dB over the entire tuning range.
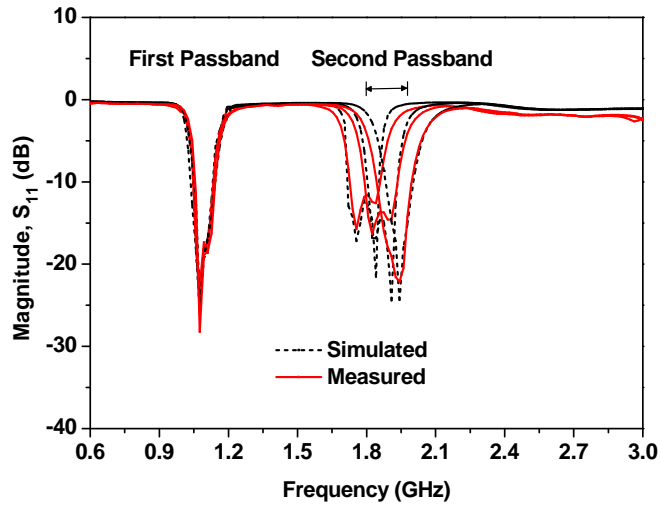
(a)
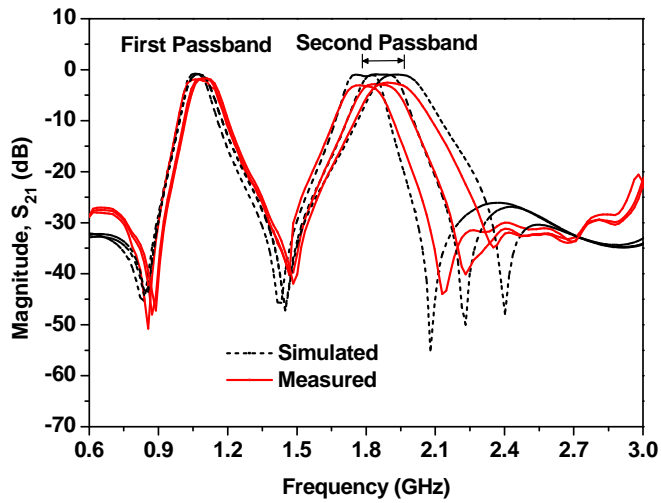
(b)

Fig. 4.14. Simulation and measurement result of filter VII with fixed first passband and tunable second passband : (a) return loss and (b) insertion loss characteristics. Reverse bias voltage variation : V_{Cv1}=5.60 V and V_{Cv2}=4.2~15 V.

In order to verify the harmonic suppression characteristics of filter VII, the broadband harmonic suppression characteristics are shown in Fig. 4.15. The harmonic suppression characteristics of the fabricated filter VII are better than 20

dB up to 18 GHz for the entire tuning range of the passbands. This means that the proposed structure can suppress more than the 10th order harmonics of the second passands due to band-rejection characteristics of DGS. This confirmed that the proposed method can achieve broadband harmonic suppression without degrading its passbands performances. The photographs of the fabricated filter VII are shown in Fig. 4.16.
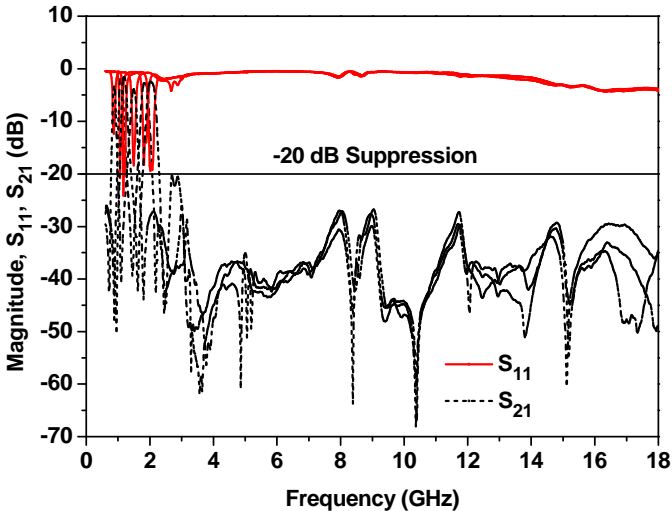
Fig. 4.15. Measured broadband harmonic suppression characteristics of filter VII in overall tuning range passbands.

(a)   (b)
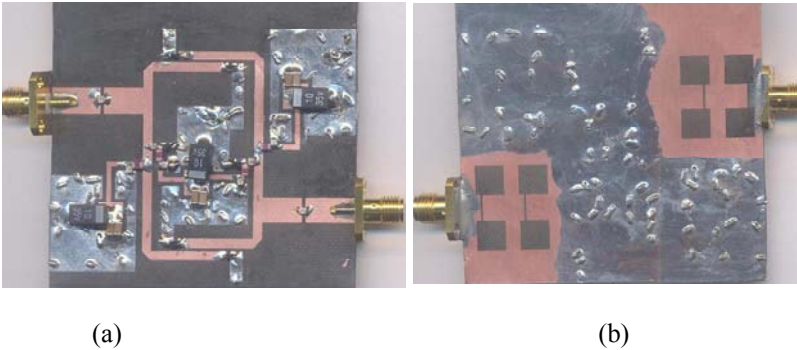
Fig. 4.16. Photograph of fabricated filter VII : (a) top side and (b) bottom side.

Fig. 4.17 presents the measured power handling capability of the proposed filter. From the measurement, it was found that the proposed filter can handle 7-12 dBm of signal level without any distortion in the passbands. The input third-order inter-modulation intercept point (IIP3) is measured around 1 GHz and 2.14 GHz with 1-MHz of 2-tone spacing. The measured IIP3s are around 24 dBm and 29 dBm at 1 GHz and 2.14 GHz, respectively. However, these values of IIP3 are not sufficient to use in practical mobile communication. Moreover, the non-linearity characteristics of proposed filter such as IIP3 can be improved by using the high Q-value varactor diodes.
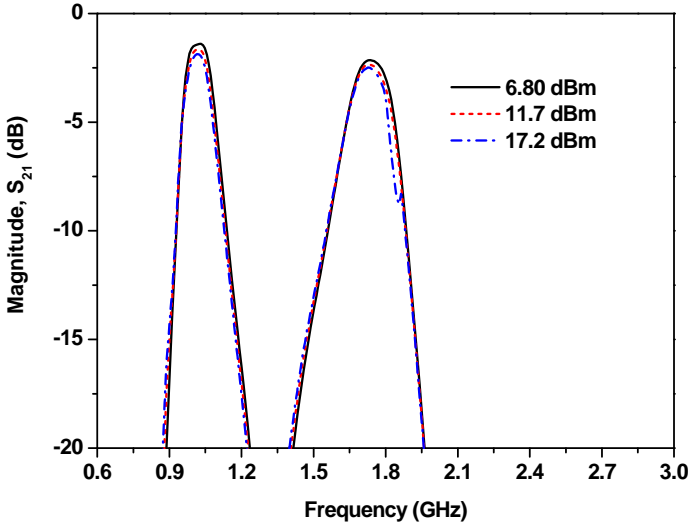
Fig. 4.17. Measured S_{21} with different input powers at bias voltages: V_{cv1}=3.7 V and V_{cv2}=3.5 V.

Performance comparisons of the proposed harmonic suppressed tunable dual-band filter with other tunable filters reported in the literature are summarized in Table 4.4.

TABLE 4.4. PERFORMANCE COMPARISON AMONG HARMONIC SUPPRESSED TUNABLE BANDPASS FILTERS.

	Frequency Tunablity [GHz]		3-dB FBW [%]	f_{c-min} [GHz]	Frequency Tuning Range [%]		Insertion Loss [dB]	Harmonic Suppression Order
	f_1=1st Passband	f_2=2nd Passband			f_1	f_2		
[35]	1.875-2.125	x	5.41	1.875	12.5	x	x	x
[37]	0.85-1.40	x	5.4*	0.85	48.88	x	1.18-3.47	x
[38]	0.6-1.03	x	2.90	0.6	41.74	x	up to 2	x
[40]	1.5-2.2	x	2.2-12.2	1.5	37.83	x	3.10-6.50	x
[41]	33.6-36/48.1-52.1	x	8.7-9.5	33.6/48.1	6.89	x	4.9-7.6	x
[42]	0.98-3.48	x	1.1	0.98	112.1	x	up to 3.57	x
[43]	Fixed @1.15	2.12-2.51	10.3/15.50	1.15/2.12	x	16.8	1.9-3.6	x
[44]	Fixed @2.43	5.28-5.74	13.58/8.6	2.43/5.28	x	8.38	1.8/2.3-4.5	x
[46]	2.20-2.7	3.45-4.20	x	2.20/3.45	20.40	19.61	up to 6	-20dB up to 1.75f_{2-max}
[50]	0.94-1.44	x	9.5	0.94	42.01	x	1.60-3.90	-15 dB up to 4f_{1-max}
This work	**0.85-1.20**	**1.40-2.14**	**13/11**	**0.85/1.40**	**34.14**	**41.80**	**1.32-3.4/1.8-3.8**	**-20 dB more than to 10f_{2-max}**

* = 1-dB FBW
f_{c-min}= Lowest passband center frequency
f_{1-max}= Highest center frequency of first passband
f_{2-max}= Highest center frequency of second passband

To facilitate a fair comparison between tunable filters, different characteristics such as insertion loss, tuning range, harmonic characteristics should be considered. The tuning range is defined by capability of filter to tune desired characteristics like center frequency whose value should be high as possible. The frequency tuning

range of filter is calculated as

$$\text{Frequency tuning range} = \frac{f_{\max} - f_{\min}}{(f_{\max} + f_{\min})/2} \qquad (4.9)$$

where $f_{\max}$ and $f_{\min}$ are maximum and minimum value of frequency, respectively. The proposed filter can provide the tunable dual-band passbands characteristics with broader frequency tunability than previously reported filters. Also, the simultaneous dual-band frequency tuning and the only second band frequency tuning are obtainable in addition to broadband harmonic rejection characteristics.

4.5   Summary and Discussion

In this chapter, the design method for harmonic suppressed tunable dual-band bandpass filters are demonstrated. Both the theoretical analysis and experiments are described to validate the proposed design method. The defected ground structures are utilized to reject harmonics. The experimental results show good agreement with the theoretical predictions. The experimental results showed that the first passband can be tuned within 34.1 % frequency tunability ratio from 0.85 to 1.2 GHz and the second passband within 41.8 % frequency tunability ratio from 1.40 to 2.14 GHz with the constant fractional bandwidth and passband shape. The proposed method can suppress more than 10th order harmonics of second passbands, thereby ensuring broadband rejection characteristics without any degradation of passband characteristics. For all the tuning states, transmission zeros are realized near the passband frequencies, which provides the high selectivity of the filter. The proposed filter design method can be applicable to selectable multi-mode or multi-band applications.

CHAPTER 5

DUAL-BAND BANDPASS FILTER WITH INDEPENDENTLY TUNABLE CENTER FREQUENCIES AND BANDWIDTHS

Some applications in wireless communication systems require tunable center frequencies and bandwidths simultaneously. In comparison to design of tunable filters, only a limited number of efforts have been made in designing filters with tunable center frequencies and bandwidth independently [51]-[53]. However, none have addressed the design of dual-band BPF with independently tunable center frequency and bandwidths.

This chapter presents a novel approach to the design of tunable dual-band BPF with independently tunable passband center frequencies and bandwidths. The newly proposed dual-band filter principally comprises two dual-mode single band filters using common input/output lines. Each single band BPF is realized using a varactor loaded transmission line dual-mode resonator. The proposed filter also offers switchable characteristics to select either of the passbands (either the first or the second passband only).

5.1 Theory and Design Equations

Fig. 5.1 shows the proposed two-pole varactor-tuned dual-band BPF. It consists of two single band BPFs combined with common input and output ports. Each single band BPF comprises dual-mode resonators that contain a transmission line and three varactor diodes. The coupling scheme of the proposed filter is shown in

Fig. 5.2, where S and L denote input and output ports. Nodes 1 and 3 denote the odd-modes and nodes 2 and 4 denote the even-modes at the first (f_1) and second passband (f_2) center frequencies, respectively. Since these two operating modes do not couple to each other, a simple tuning scheme can be obtained.
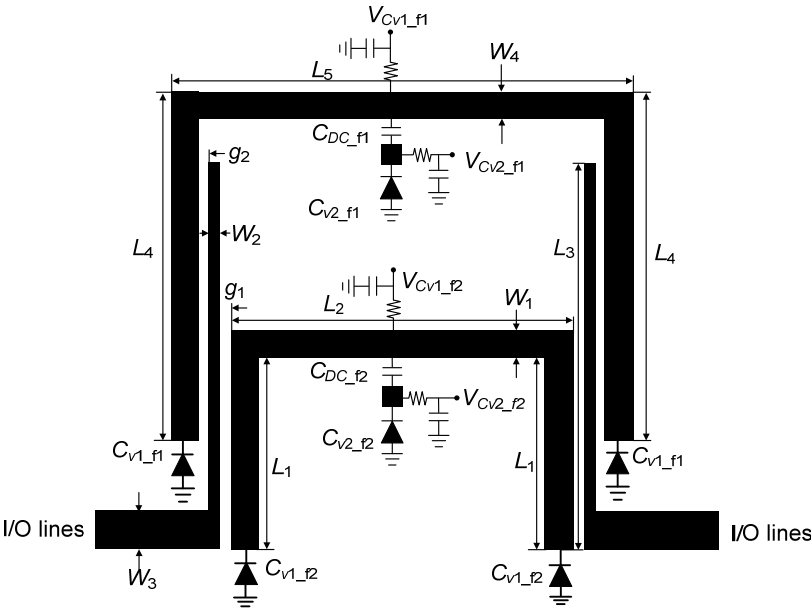
Fig. 5.1. Layout of the proposed two-pole dual-band tunable filter VIII.
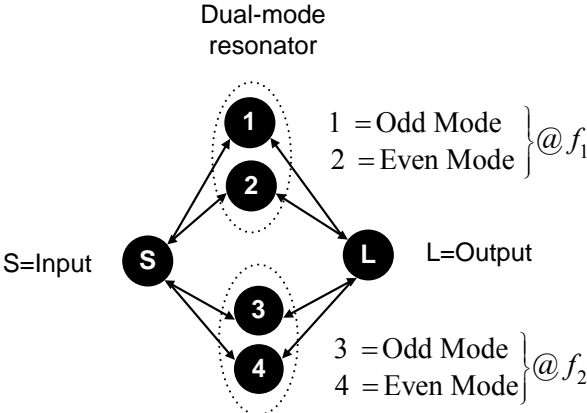
Fig. 5.2. Coupling scheme of the proposed filter VIII.

5.1.1 Characteristics of Proposed Resonator

Fig. 5.3 shows the basic structure of the proposed resonator. Two varactor diodes are attached at the ends of the transmission line with tunable capacitances C_{v1} and one varactor diode with tunable capacitance C_{v2} is attached at the center point of transmission line. The DC block capacitor is placed at the center point of the transmission. For the theoretical analysis, the lossless transmission line of characteristic admittance Y and physical length L is assumed. Since the structure is symmetrical, the even- and odd-mode analysis method is applicable to obtain the resonant frequencies. When the odd-mode excitation is applied to the ends of the proposed resonator shown in Fig. 5.3(a), there is a voltage null along the symmetry plane. Under the odd-mode excitation, it can be represented by the half circuit as shown in Fig. 5.3(b). The odd-mode input admittance is given as follows.

$$Y_{in\_odd} = j\left[\omega_{odd}C_{v1} - Y\cot\left(\beta L/2\right)\right] \tag{5.1}$$

Where C_{v1} is the capacitance of the varactor diode connected at the end of the line and β is the propagation constant of the transmission line. From the resonance condition of $\text{Im}(Y_{in\text{-odd}})=0$, the odd-mode resonant frequency can be determined as follows.

$$f_{odd} \times \tan\left(\frac{\pi f_{odd} L}{v_p}\right) = \frac{Y}{2\pi C_{v1}} \tag{5.2}$$

Where v_p is the phase velocity. From (5.2), it is concluded that the odd-mode resonant frequency fully depends on the capacitance C_{v1} of varactor diode
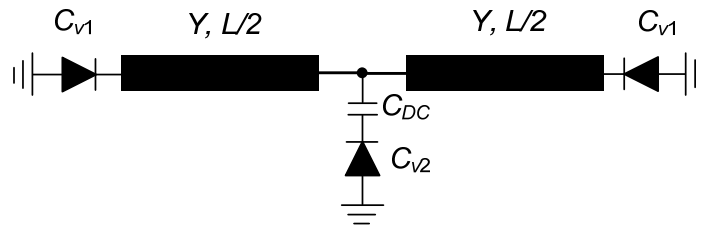
(a)
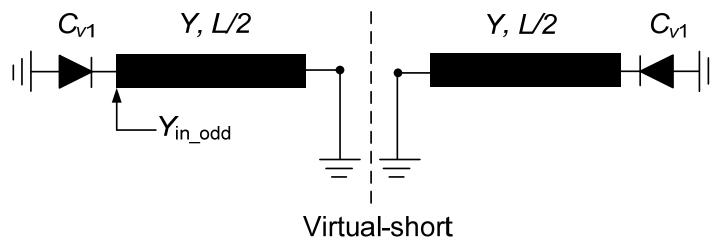
(b)
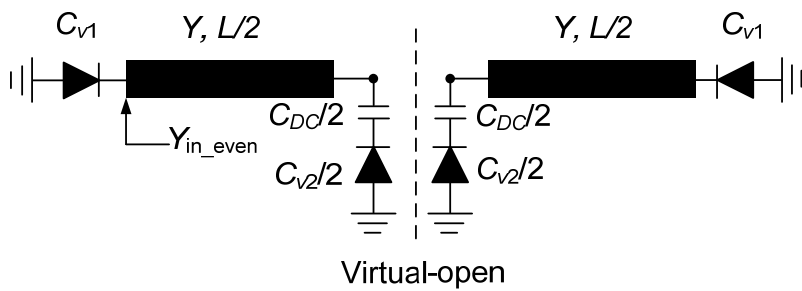
(c)

Fig. 5.3. (a) Basic structure of the proposed resonator, (b) odd-mode excitation equivalent circuit, and (c) even-mode excitation equivalent circuit.

connected at the ends of the transmission line. Moreover, the odd-mode resonant frequencies are not affected by the varactor diode connected at the center of the transmission line.

For the even-mode excitation, there is no current flowing through the center of the transmission line. Under the even-mode condition, the proposed resonator can be represented by the equivalent half circuit shown in Fig. 5.3(c). The even-mode input admittance is given as follows.

$$Y_{in\_even} = j\left(\omega_{even} C_{v1} + Y \frac{\omega C_{v2\_t} + Y \tan\left(\beta L/2 \right)}{Y - \omega \tan\left(\beta L/2 \right) C_{v2\_t}} \right) \tag{5.3}$$

Where C_{v2_t} is the total capacitance for series connection of dc block capacitor and varactor diode, which is given as follows.

$$C_{v2\_t} = \frac{1}{2} \frac{C_{v2} C_{DC}}{C_{v2} + C_{DC}} \tag{5.4}$$

Where C_{v2} and C_{DC} are the capacitance of the varactor diode and dc block connected at the center of the transmission line, respectively. For the resonance condition, the even-mode resonant frequency can be determined as follows.

$$\left(f_{even} - \frac{Y^2}{4\pi^2 f_{even} C_{v1} C_{v2\_t}} \right) \tan\left(\frac{\pi f_{even} L}{v_p} \right) = Y \frac{C_{v1} + C_{v2\_t}}{2\pi C_{v1} C_{v2\_t}} \tag{5.5}$$

From (5.4) and (5.5), it can be observed that the even-mode resonant frequency depends on C_{v1} and C_{v2}. Moreover, when C_{v1} is fixed, the even-mode resonant

frequency can be tuned with C_{v2} alone. This characteristic of the proposed resonator can be used to the design of BPF with the tunable bandwidths.

In order to verify the theoretical analysis, a full-wave electromagnetic (EM) simulation was carried out using HFSS v11 of Ansoft and resonant characteristics of proposed resonator is shown in Fig. 5.4. Two microstrip lines with characteristic impedance of 50 Ω were utilized to feed the proposed resonator using loose coupling to investigate its resonant behavior. The characteristic impedance of resonator are fixed at 76 Ω.

Fig. 5.4 shows the simulated S_{21}-magnitude of weak coupling resonator circuit according to different capacitances (C_{v1} and C_{v2}) of varactor diodes and length (L). As C_{v1} and C_{v2} are varied, the odd- and even-mode resonant frequencies are tuned simultaneously. This characteristic of the proposed resonator can be utilized in the design of BPF with tunable passband center frequency. If capacitances C_{v1} of the varactor diodes connected at the end of the transmission line are fixed, it is obvious that the odd-mode resonant frequency is fixed and the even-mode resonant frequency can be tuned by varying the capacitance C_{v2} of the varactor diode connected at the center of the line. The separation between the modal frequencies is proportional to the bandwidth. This characteristic of proposed resonator can be utilized in the design of BPF with tunable bandwidths.

5.1.2 External Quality Factor (Q_e)

With input/output coupling, the circuit models for the odd- and even- modes are presented in Fig. 5.5. The odd- (Q_{exo}) and even-mode (Q_{exe}) external quality factor

of the proposed filter can be derived from the input reflection coefficient of the
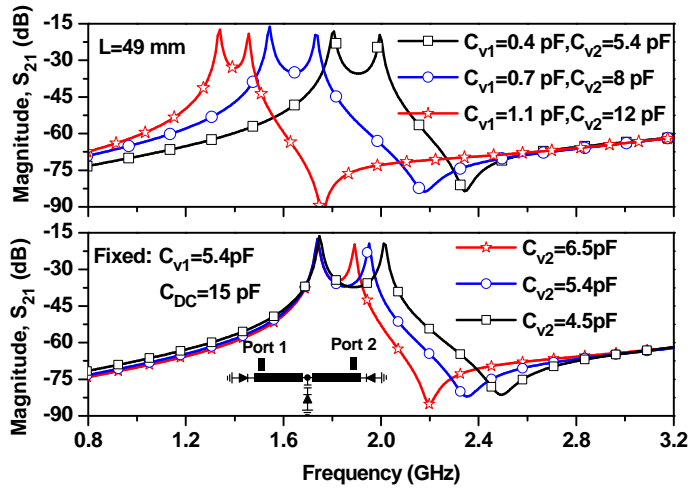
(a)
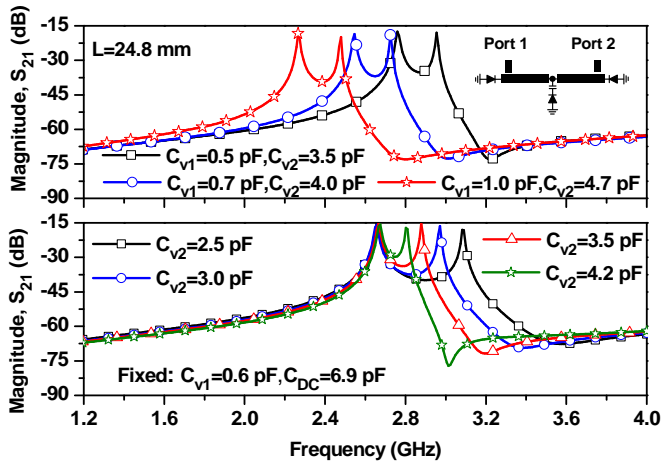
(b)

Fig. 5.4. Resonant frequencies of single dual-mode resonator according to capacitances and length

at : (a) first passband and (b) second passband.
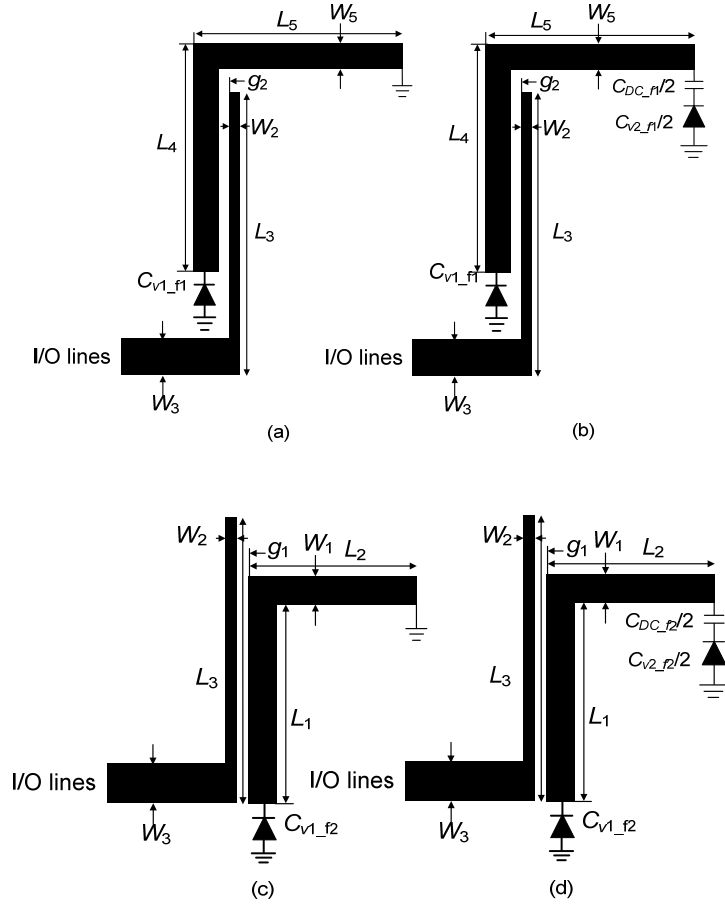
Fig. 5.5. Circuit model of (a) odd-mode at first band, (b) even mode at first passband, (c) odd-mode at second band, and (d) even-mode at second passband with I/O coupling.

odd- and even-modes [38] as follows.

$$Q_{exo} = \pi f_{odd} \tau_{S11\_odd} \tag{5.6a}$$

$$Q_{exe} = \pi f_{even} \tau_{S11\_even} \tag{5.6b}$$

Where $\tau_{s11\text{-}odd}$ and $\tau_{s11\text{-}even}$ are group delays of S_{11} at the odd- and even-modes resonant frequencies, respectively.

Fig. 5.6 shows the extracted external quality factors for the first and second passbands under different g_1 and g_2 gaps between resonator and input/output (I/O) lines. As g_1 and g_2 are increased, the external quality factors also increased. To maintain the shape and bandwidth of odd- and even-mode frequency responses, the external quality factors for the odd- and even-mode should vary with tuning frequency.
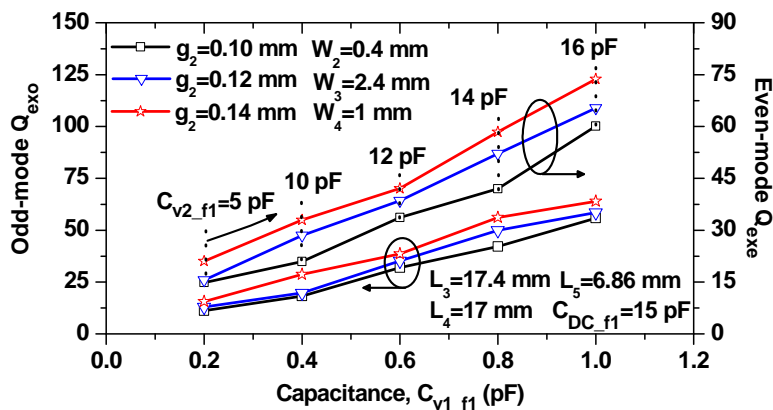
(a)
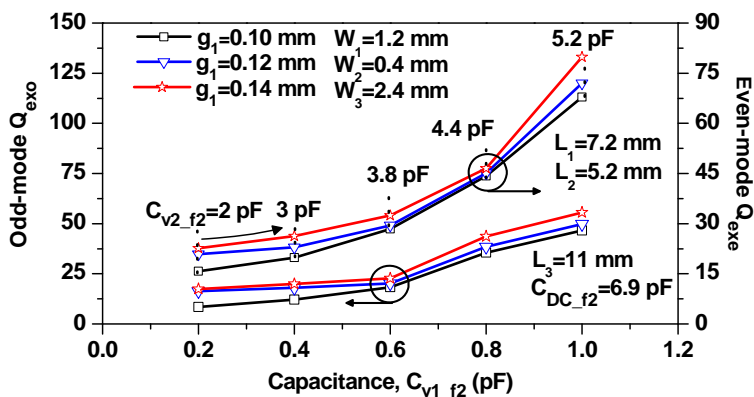
(b)

Fig. 5.6. Extracted external quality factors at (a) first passband and (b) second passband. Refer to Fig. 5.5 for notation.

As seen from Fig. 5.6, the odd-mode external quality factor can be controlled by C_{v1} only, whereas the even-mode external quality factor can be varied by both C_{v1} and C_{v2}. Therefore, from these graphs, values of g_1, g_2 and L_3 can be determined to meet the design specifications of filter.

5.1.3   Design Method

Firstly, it should be determined the requirement of the ideal dual-mode tunable filter at each passband which may be derived from its fixed frequency response centering at the high-frequency edge of the given tuning range. Then separation of odd- and even-mode resonant frequencies and the required Q_{exo} and Q_{exe} for the ideal tunable filter can be determined at each passband as described in [38]. Secondly, tuning rate of the odd-and even-mode resonant frequencies should be determined by selecting Y, L, C_{v1}, and C_{v2} by using (5.2) and (5.5) at each passband separately. Thirdly, the coupling network should be designed to maintain the shape and bandwidth of odd- and even-mode frequency responses over the tuning range by properly choosing g_1, g_2 and L_3 according to the ideal requirement of filter response.

To demonstrate the described design method, the filter centering at f_1=1.80 GHz and f_2=2.9 GHz with 3-dB FBWs of 5.8 % and 9.5% has been designed, respectively. The desired parameters can be derived from a target coupling matrix corresponding to specified response [58], which are given as $f_{odd\text{-}f1}$=1.74 GHz, $f_{even\text{-}f1}$=1.94 GHz, $Q_{exo\text{-}f1}$=20.5 and $Q_{exe\text{-}f1}$=40.2 at the lower passband (f_1) and $f_{odd\text{-}f2}$=2.76 GHz, $f_{even\text{-}f2}$=3.04 GHz, $Q_{exo\text{-}f2}$=23.5 and $Q_{exe\text{-}f2}$=29.5 at the higher passband (f_2).

With these design parameters, length and characteristic impedance of resonators at the first (f_1) and second (f_2) passband are chosen as 51 mm, 24.8 mm, and 76 Ω, respectively. Also according to the external quality factors, value of g_1, g_2, W_2, and L_3 are taken as 0.12 mm, 0.14 mm, 0.4 mm, and 17.5 mm from Fig. 5.6, respectively.

5.1.4 Analysis of Center Frequency and Bandwidth Tunability

To tune the center frequency with constant filter response and bandwidth, two factors must be considered. Firstly, the resonant frequencies of odd- and even-modes should be shifted proportionally. Secondly, the external quality factors for the odd and even-modes should vary directly with tuning frequency. Similarly, the separation between the odd-and even-modes resonant frequencies are proportional to the bandwidth tunability while keeping the center frequency of passbands constant. Therefore, the filter bandwidth can be tuned by properly tuning the value of C_{v2} while keeping constant value of C_{v1}. To demonstrate how to achieve these, the simulated results are plotted in Fig. 5.7.

Fig. 5.7(a) presents tunability of center frequency of passbands according to capacitances ($C_{v1\text{-}f1}$, $C_{v2\text{-}f1}$, $C_{v1\text{-}f2}$, and $C_{v2\text{-}f2}$). The first passband center frequency (f_1) can be tuned from 1.4-1.82 GHz by adjusting $C_{v1\text{-}f1}$ from 0.4-0.9 pF and $C_{v2\text{-}f1}$ from 5.1-10.2 pF. Similarly, the second passband center frequency (f_2) can be varied from 2.26-3 GHz by changing $C_{v1\text{-}f2}$ from 0.4-0.9 pF and $C_{v2\text{-}f2}$ from 2.2 to 6.7 pF.

Fig. 5.7(b) presents the 3-dB FBWs versus capacitances (fixing $C_{v1\text{-}f1}$ and $C_{v1\text{-}f2}$

and varying $C_{v2\text{-}f1}$ and $C_{v2\text{-}f2}$) for f_1=1.53-1.82 GHz and f_2=2.38-3 GHz. From the simulation, it is found that the 3-dB FBW results in tunable range of 5-9 % for f_1=1.53-1.82 GHz and 6-12 % for f_2=2.38-3 GHz.
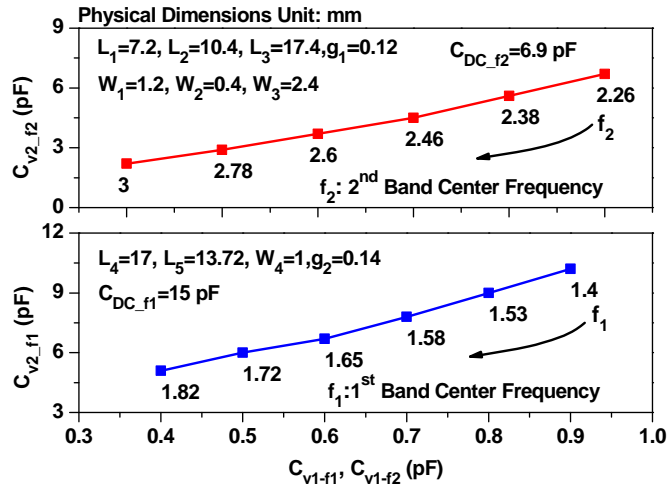
(a)
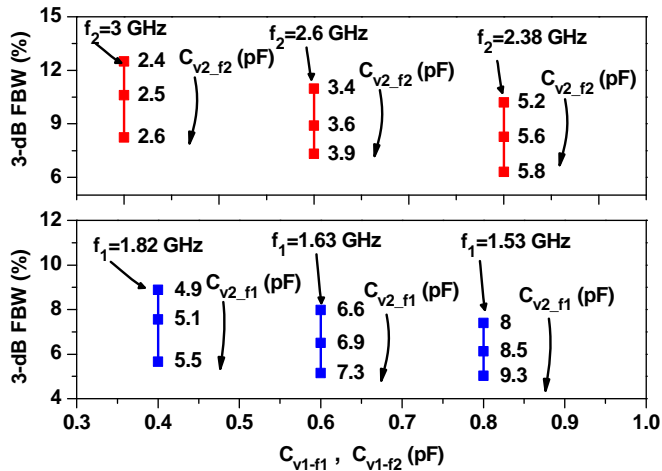
(b)

Fig. 5.7. Simulated results for tunability of center frequency and bandwidths of passbands according to capacitances : (a) passbands center frequency tunability and (b) bandwidths tunability. Refer to Fig. 5.1 for notation.

TABLE 5.1. DIMENSIONS FOR FABRICATED FILTER VIII (DIMENSIONS ARE IN MILIMETERS), REFER TO FIG. 5.1 FOR NOTATION.

$W_1/W_2/W_3/W_4$	$L_1/L_2/L_3/L_4/L_5$	g_1/g_2	C_{DC_f1}/C_{DC_f2} [pF]
1.2/0.4/2.4/1	7.2/10.4/17.4/17/13.72	0.12/0.14	15/6.9

5.2 Filter Implementation and Verification

To verify the analytical analysis of the proposed resonators, two types of tunable dual-band BPF were designed, simulated and measured. Fig. 5.1 depicts the configuration of microstrip dual-mode tunable dual-band filter VIII. In the proposed filter, two dual-mode resonators are combined with common input/output ports. The inner resonators are designed for the higher passbands, whereas the outer resonator is designed for the lower passpbands. The resonators are folded in order to reduce the size. The substrate is RT/Duriod 5880 made by Rogers with dielectric constant (ε_r) of 2.2 and thickness (h) of 31 mils.

The proposed filter employs two type of varactor diodes from Skyworks: SMV1231-011LF for tuning C_{v1-f1} and C_{v1-f2} and SMV1233-079LF for tuning of C_{v2-f1} and C_{v2-f2}, respectively. After the simulation, the physical parameters and component values of the filter were determined, as shown in Table 5.1.

5.2.1 Filter VIII: Tunable Center Frequencies

Fig. 5.8 shows the simulation and measurement results of filter VIII for several typical bias voltages. The measurement results agree well with the simulation

results. The measurement results show that the first passband center frequency can be tuned from 1.48 to 1.8 GHz and the second passband center frequency can be tuned from 2.40 to 2.88 GHz. The return loss is better than 12 dB in the overall tuning range of both passbands. The insertion loss varies from 1.99 to 4.4 dB at the first passband, whereas it varied 1.60 to 4.2 dB at the second passband. As the passbands are tuned towards the lower frequencies, the insertion loss becomes higher because the Q value of varactors becomes lower at around low bias voltages.
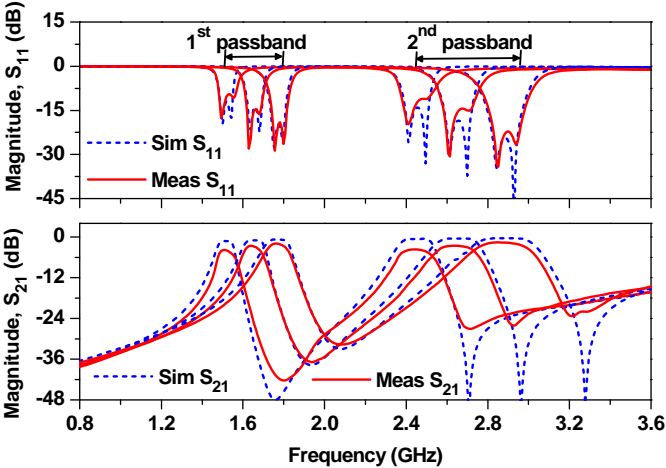
Fig. 5.8. Simulation and measurement results of filter VIII with tunable both passbands. Bias voltage variation : V_{Cv1_f1}=3.78~15 V, V_{Cv2_f1}=0.59~15 V, V_{Cv1_f2}=4~15 V, and V_{Cv2_f2}=4~15 V.

Fig. 5.9 shows the simulation and measurement results of filter VIII with the fixed second passband and tunable first passband center frequencies. The second passband center frequency is fixed at 2.88 GHz and the first passband center frequency is tuned from 1.48 to 1.8 GHz. The return loss is better than 12 dB over

the entire tuning range of first passband. The insertion loss varies from 1.99 to 4.42 dB.
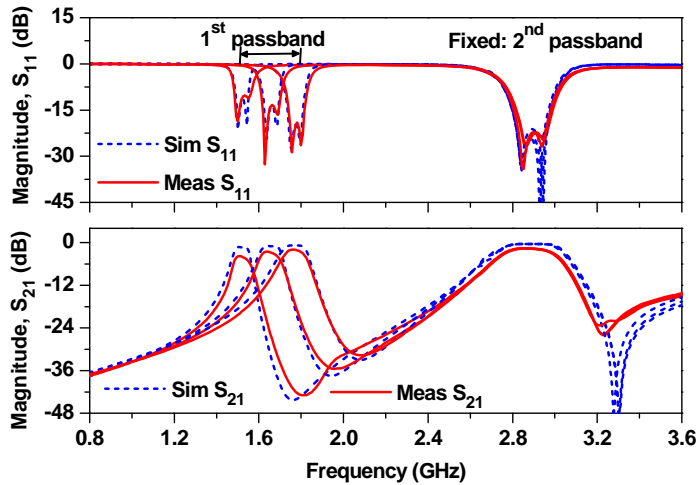
Fig. 5.9. Simulation and measurement results of filter VIII with tunable first passband and fixed second passband. Bias voltage variation : V_{Cv1-f1}=3.78~15 V, V_{Cv2-f1}=0.59~15 V, V_{Cv1-f2}=15 V, and V_{Cv2-f2}=15 V.

Fig. 5.10 shows the simulation and measurement results of filter VIII with the fixed first passband and tunable second passband center frequencies. The first passband center frequency is fixed at 1.74 GHz, and the second passband center frequency is tuned from 2.40 to 2.88 GHz with the return loss better than 12 dB over the entire tuning range. The insertion loss varies from 1.64 to 4.2 dB. From these results, it is clear that center frequencies of proposed filter can be tuned independently. However, the differences in insertion loss between the simulation and measurement results are due to the use of ideal capacitances in EM simulation.
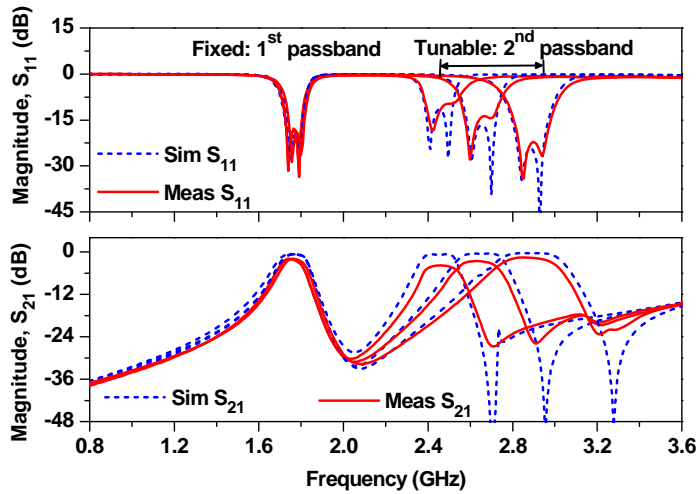
Fig. 5.10. Simulation and measurement results of filter VIII with fixed first passband and tunable second passband. Bias voltage variation : $V_{Cv1\text{-}f1}$=15 V, $V_{Cv2\text{-}f1}$=15 V, $V_{Cv1\text{-}f2}$=4~15 V, and $V_{Cv2\text{-}f2}$=4~15 V.

5.2.2 Filter VIII: Tunable Bandwidths

Fig. 5.11 shows the simulation and measurement results of filter VIII with both tunable passband bandwidths. As seen in this figure, the first passband 3-dB FBWs can be tuned from 5.76 to 8.55 % at the center frequency of 1.74 GHz and the second passband 3-dB FBW variation from 8.28 to 12.42 % at the center frequency of 2.80 GHz, respectively. Fig. 5.12 and 5.13 show the simulation and measurement results of filter VIII to verify independently the tunable 3-dB FBWs of passbands. As seen in the Fig. 5.12, the 3-dB FBW of the first passband is tunable with the fixed second passband bandwidth. Similarly, Fig. 5.13 shows the

simulation and measurement results for the tunable 3-dB FBWs of the second

passband with the fixed first passband bandwidth.

(a)

(b)

85
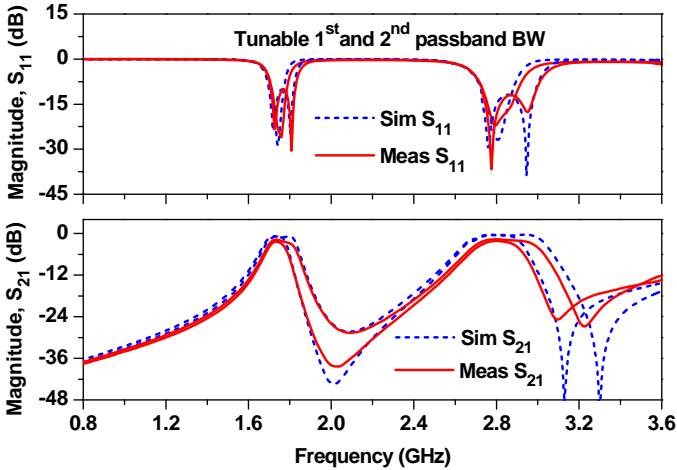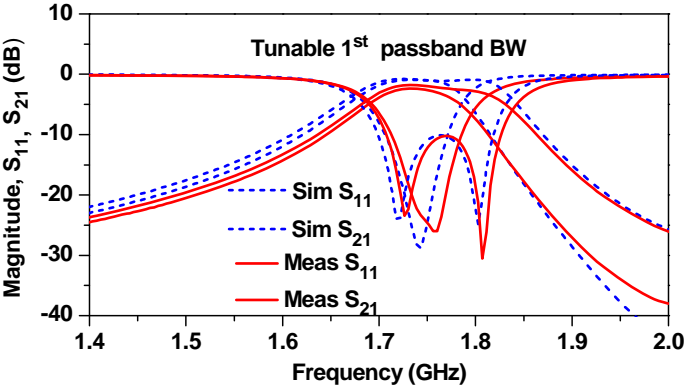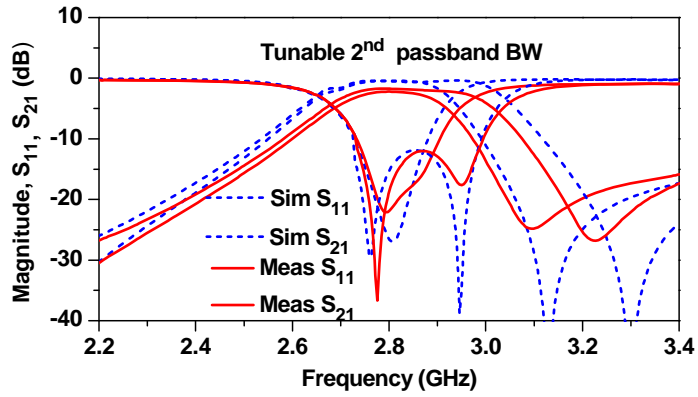
(c)

Fig. 5.11. Simulation and measurement results of filter VIII with tunable bandwidth of both passbands simultaneously. (a) Both passbands, (b) expanded first band characteristics, and (c) expanded second band characteristics. Bias voltage variation : V_{Cv1-f1}=15 V, V_{Cv2-f1}=6~15 V, V_{Cv1-f2}=15 V, and V_{Cv2-f2}=8~15 V.
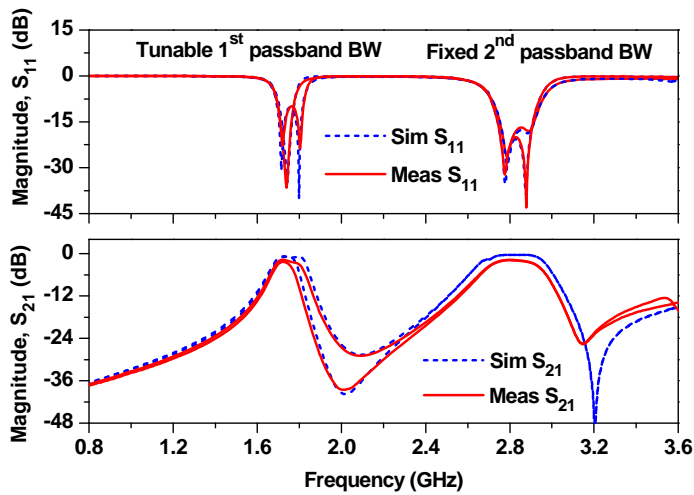
(a)
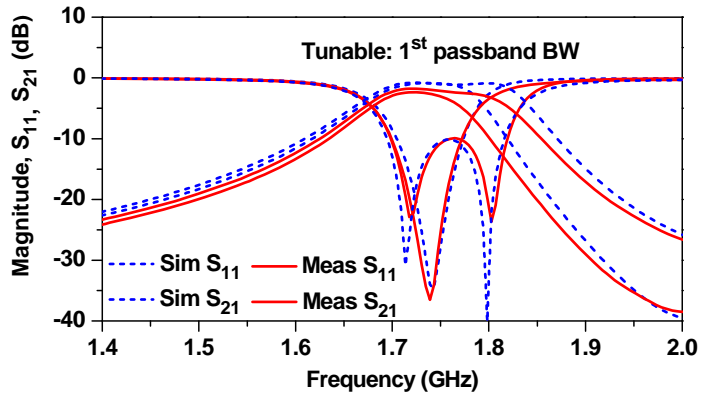
(b)

Fig. 5.12. Simulation and measurement results of filter VIII with fixed second passband bandwidth and tunable first passband bandwidth : (a) both passbands, and (b) expanded first band characteristics. Bias voltage variation: V_{Cv1_f1}=15 V, V_{Cv2-f1}=6~15 V, V_{Cv1-f2}=15 V, and V_{Cv2-f2}=15 V.
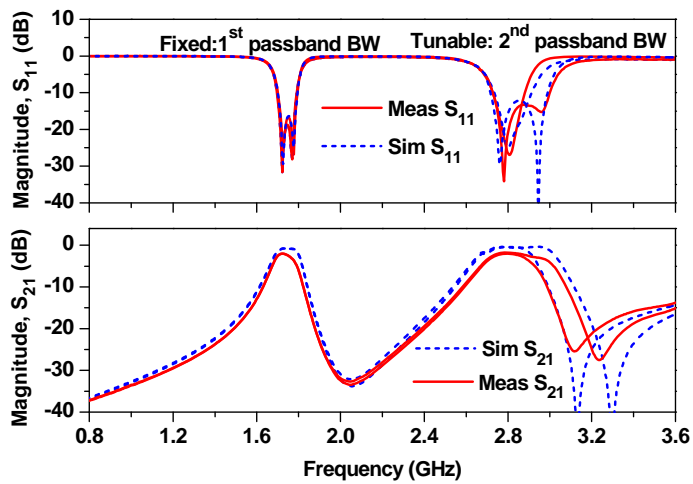
(a)
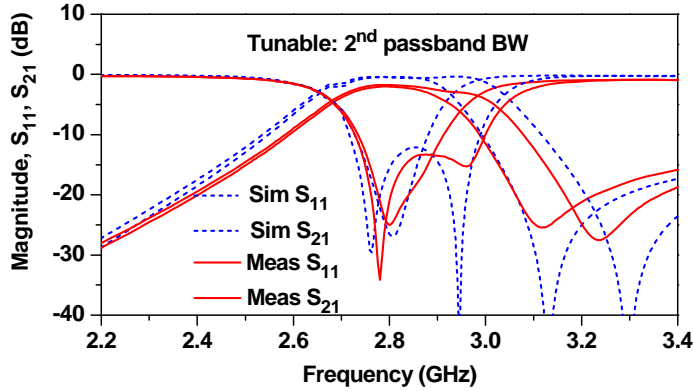
(b)

Fig. 5.13. Simulation and measurement results of filter VIII with fixed first passband bandwidth and tunable second passband bandwidth : (a) both passbands and (b) expanded second band characteristics. Bias voltage variation : V_{Cv1_f1}=15 V, V_{Cv2-f1}=15 V, V_{Cv1-f2}=15 V, and V_{Cv2-f2}=8~15 V.

5.2.3   Filter VIII: Passband Switchable Characteristics

The proposed filter also offers the switchable passband characteristics, as shown in Fig. 5.14. By varying the capacitances of varactor diodes, either only the first or the second passband can be selected. The first passband can be only selected by tuning the second passband odd- and even-mode resonant frequencies toward lower frequencies. Similary, the second passband can be only selected by tuning the first passband odd- and even-mode resonant frequencies toward lower frequencies. However, the complete removal of passband could not be performed because the varactor diode capacitances were not high enough as the required theoretically. While tuning odd- and even-mode resonant frequencies toward lower frequencies, the required coupling coefficient and external quality factors can not be obtained

88

which eliminates the passbands. The photograph of fabricated filter VIII is shown in Fig. 5.15.
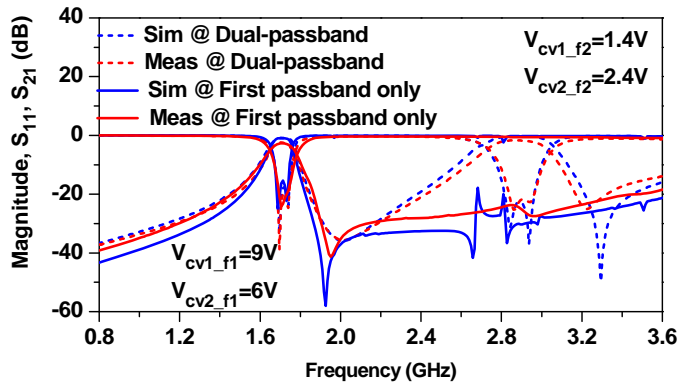
(a)
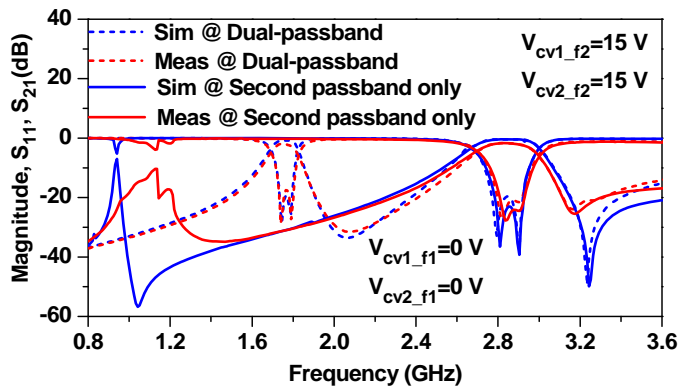
(b)

Fig. 5.14. Simulation and measurement results of filter VIII with passband switchable characteristics : (a) only first passband and (b) only second passband.
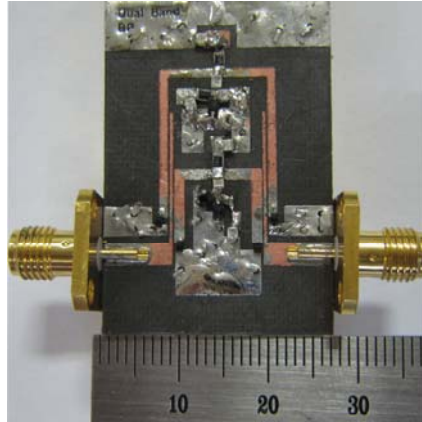
Fig. 5.15. Photograph of fabricated filter VIII.

5.2.4 Filter IX: Tunable Dual-band Bandpass Filter with Harmonic Suppression

It can be found from the simulation and measurement results in the previous section that there are several harmonics of the two passbands. These harmonics are also tuned by varying the passband frequencies and must be suppressed for improving the overall system performances.

Fig. 5.16 shows the proposed configuration of the harmonic suppressed tunable dual-band filter IX. In this structure, the DGS is used at the input/output feeding transmission lines for inducting coupling and acts as the broadband rejection resonator to suppress the harmonics of filter VIII. The physical parameters and component values of the filter IX are shown in Table 5.2.
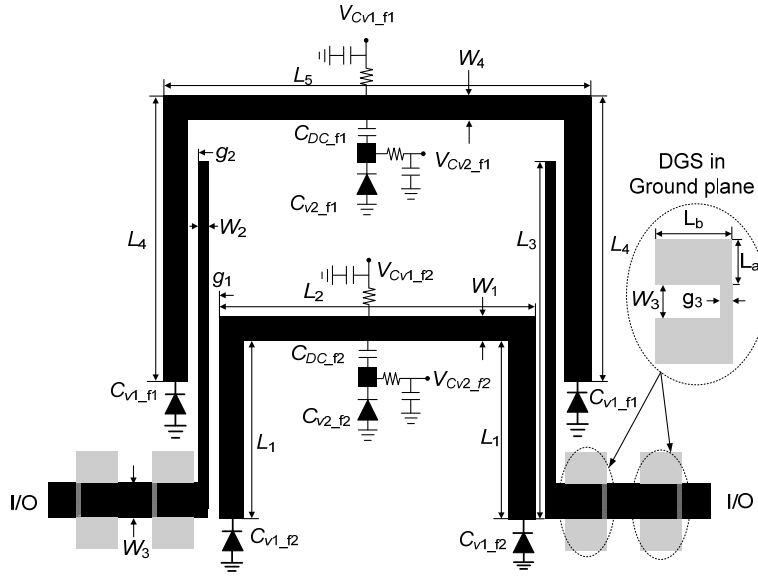
Fig. 5.16. Configuration of filter IX.

TABLE 5.2 DIMENSIONS FOR FABRICATED FILTER IX (DIMENSIONS ARE IN MILIMETERS), REFER TO FIG 5. 16 FOR NOTATION.

$W_1/W_2/W_3/W_4$	$L_1/L_2/L_3/L_4/L_5/L_a/L_b$	$g_1/g_2/g_3$	C_{DC_f1}/C_{DC_f2} [pF]
1.2/0.4/2.4/1	7.2/10.4/17.4/17/13.7/5/4	0.12/0.14/0.28	15/6.9

Fig. 5.17 (a) shows narrowband characteristics of the simulation and measurement results of filter IX. The passband frequencies are tuned with the help of the bias voltages of the varactor diodes. From the measurement results, the first passband frequency can be tuned from 1.5 to 1.8 GHz and the second passband frequency can be tuned from 2.45 to 2.80 GHz. The return loss is better than 11 dB over the entire tuning range of the passbands. The insertion loss varies from 3.02 to 4.8 dB at the first passband and 2.78 to 4.6 dB at the second passband. These

measurement results for filter IX are almost similar with filter VIII results in the previous section except for the suppression of the harmonic characteristics. In order to verify the harmonic suppression characteristics of filter IX, the broadband harmonic suppression characteristics are measured and shown in Fig. 5.17 (b).
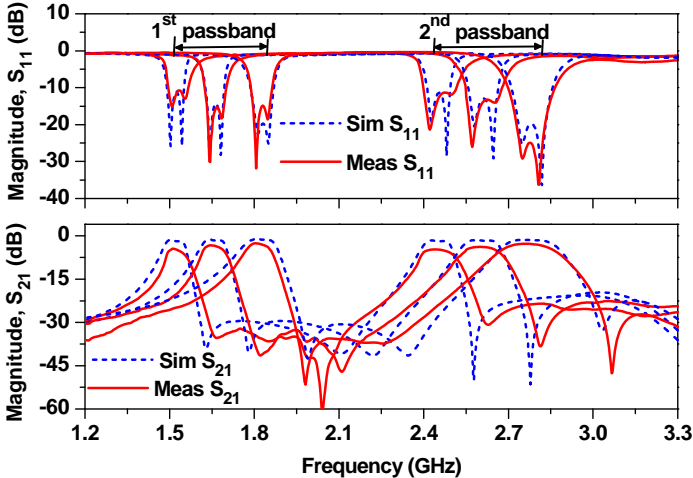
(a)
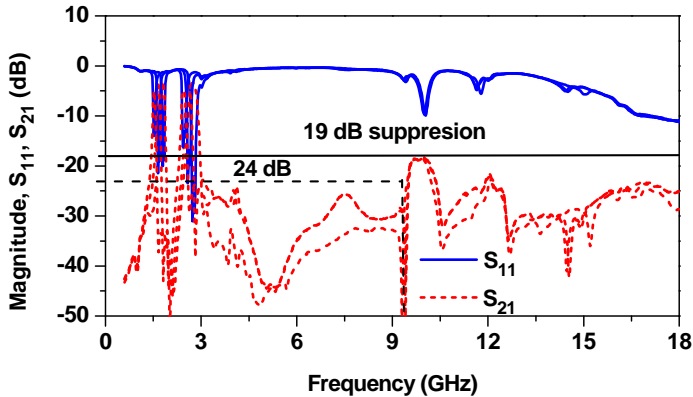
(b)

Fig. 5.17. Simulation and measurement results of filter IX with tunable both passbands : (a) narrowband and (b) wideband characteristics. Bias voltage variation : V_{Cv1_f1}=4.09~13V, V_{Cv2-f1}= 0.93~15 V, V_{Cv1-f2}=5.60~15 V, and V_{Cv2-f2}=3.21~15 V.

The harmonic suppression characteristics for the fabricated filter IX are better than 19 dB up to 18 GHz over the entire tuning range of the passbands. This means that the proposed structure can suppress more than 10th order harmonics of the highest center frequency of first passand due to the band-rejection characteristics of DGS. This confirmed that the proposed method can achieve the broadband harmonic suppression without degrading any passbands performances. The photographs of the fabricated filter IX are shown in Fig. 5.18.

(a)   (b)
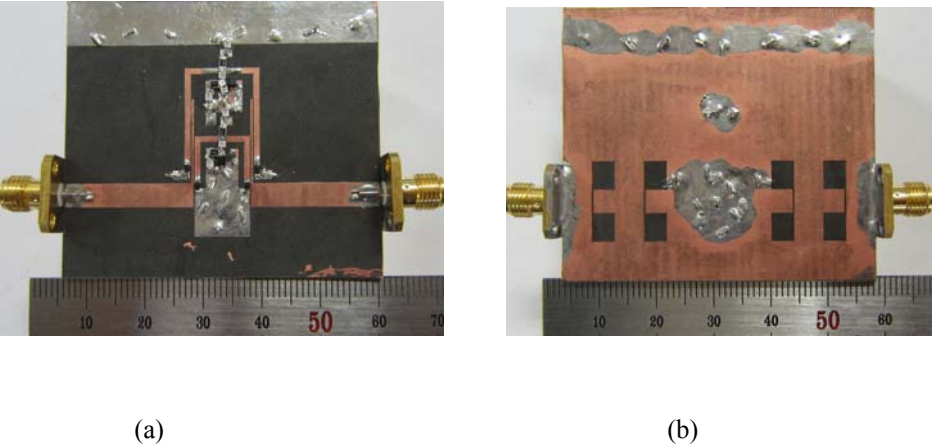
Fig. 5.18. Photograph of fabricated filter IX : (a) top view and (b) bottom view.

The performance comparisons of the proposed tunable filter with other tunable filters reported in the literature are summarized in Table 5.3. The comparison has performed considering the different characteristics such as tunability of bandwidth, insertion loss variation and so on. The proposed filter can provide the dual-passbands with the independently tuned center frequencies and bandwidths in addition to broadband harmonic rejection characteristics.

TABLE 5.3 PERFOMANCE COMPARISON OF TUNABLE FILTERS WITH INDEPENDENT CONTROL OF CENTER FREQUENCIES AND BANDWIDTHS.

	Frequency Tunability [GHz]		3-dB FBW Tunability [%]		A	Insertion Loss [dB]	Harmonic Suppression Order
	f_1	f_2	f_1	f_2			
[37]	0.85-1.40	x	2.9-5.2*	x	N	1.18-3.47	x
[40]	1.50-2.20	x	2.2-12.2*	x	Y	3.10-6.50	x
[45]	1.75-2.25	x	4-5.71*	x	Y	4.90-7.60	x
[46]	2.20-2.27	3.45-4.2	x	x	N	up to 6	-20 dB up to 1.75f_{1_max}
[47]	2.90-3.50	x	4-12	x	Y	1.0-3.0	x
[48]	0.47-0.862	x	1.06-3.19	x	Y	2.20-4.90	x
[49]	3.70-6.0**	x	1.6-9.3*	x	Y	2.10-2.20**	x
[50]	0.94-1.44	x	x	x	N	1.60-3.90	-15 dB up to 4f_{1_max}
This work	**1.48-1.80**	**2.40-2.88**	**5.7-8.5**	**8.2-12.4**	**Y**	**1.99-4.4/1.6-4.2**	**-19 dB more than to 10f_{1_max}**

A= Independently tunable center frequency and bandwidth
Y/N=Yes/No
*=1-dB FBW
**=Suspended-striplinerings in MEMS technology
f_{1_max}= Highest center frequency of first passband
f_{2_max}= Highest center frequency of second passband

5.3   Summary and Discussion

In this chapter, the design of tunable dual-band bandpass filters with independently tunable center frequencies and bandwidths are demonstrated. The proposed structure is validated by both theoretical analysis and experiments. The defected ground structures are utilized to reject harmonics. The experimental results are in good agreement with the theoretical predictions. The experimental

results showed that the first passband can be tuned from 1.48 to 1.8 GHz with the 3-dB fractional bandwidth tunability of 5.76 to 8.55 % and the second passband from 2.40 to 2.88 GHz with the 3-dB fractional bandwidth tunability of 8.25 to 12.42 %. The proposed filter also offers passband switchable characteristics. The proposed method can suppress more than 10th order harmonics of second passbands, thereby ensuring the broad harmonic rejection characteristics without any degradation of passband characteristics. The proposed filter design method can be applicable to selectable multi-mode or multi-band applications that have different operating frequencies and bandwidths. The proposed filter topology is simple to implement and a good candidate for communication system requiring multi-band tunable filter with center frequency and bandwidth control.

CHAPTER 6

CONCLUSION AND FUTURE WORK

This chapter presents the conclusion of this thesis contribution and some future research directions in the area of microwave tunable multi-band filters that could be developed based on the design and synthesis method presented in this thesis.

6.1   Conclusion

Many wireless communication standards such as wireless local area networks (WLAN), world-wide interoperability for microwaves (WiMax), wideband code division multiple access (WCDMA), long term evolution (LTE) etc, have been developed throughout the whole world and apparently more standards are to emerge in the near future. The integration of separate standards into one mobile unit or base-station increases the size, cost and complexity of the wireless systems. The need for the design of low-cost, compact robust radio frequency components operating at multiple frequency bands became apparent to meet the demands of next generation wireless systems.

The first key point of this thesis was understanding design and synthesis of tunable multi-band bandpass filters at microwave frequencies. The proposed goals were achieved with the original contributions presented journals and conference proceedings. These works are listed in the "publication" section in this thesis.

In chapter 2, the design of dual-band BPF with arbitrary bandwidths are presented based on new simple mapping function. The analytical design equations are derived from the lumped element prototype of the conventional low pass filters and implemented with distributed transmission lines by applying the circuit conversion techniques. The designed filters were applicable for WCDMA, WiMax, and WLAN applications.

The chapter 3 presented the application of variable characteristic impedance transmission lines for designing tunable dual-band bandpass filters. The designed filter offered the fixed first and tunable second passbands. The second passband of proposed filter was tuned by using DGS and varator diodes. The designed filter was applicable for GPS and WLAN applications.

The harmonic bands which degrade the out-of passband characteristics are also tuned with tunable passband characteristics. Thus, the suppression of harmonics is one of critical issue of tunable filters. To achieve this goal, the harmonic suppressed dual-band bandpass filters with tunable passband center frequencies is presented in chapter 4. The characteristics of dual-mode resonator based on varactor diode loaded transmission were analyzed using the odd- and even-mode analysis and their characteristics were used to the design of dual-band BPF with tunable both passbands as well as fixed first passband and tunable second passbands only.

In wireless communication systems such as cognitive radio systems, the radios themselves sense the available spectrum and decide on the communications channel (frequency, bandwidth, and modulation scheme) to use. Therefore, it is important to design the tunable multi-band filter with changing the center

frequencies and bandwidths. Thus fifth part of thesis is devoted to design dual-band BPF with independently tunable passband center frequencies and bandwidths simultaneously which is described in Chapter 5.

6.2   Future Research Direction

The methodology presented in this thesis could be applied to design the higher order dual-band/tunable filters by coupling more than one resonators as shown in Fig. 6.1 in order to achieve smaller bandwidths, higher level of out-of-band rejection and sharper cut-off slopes. The proposed filter consists of 4-dual-mode resonators which are connected using parallel feed structure. Further, the design method presented in chapter 5 of this thesis can also be expanded to the design of the triple/Quad-band bandpass filters with independently tunable passband center frequencies and bandwidths.

Current designed filters have a little large circuit size. Therefore, a size reduction is important in the view of cost and performance. Therefore, LTCC technology could be considered for this purpose.

In this thesis, tuning of designed dual-band bandpass filters were realized by varactor diodes. However other type of tuning elements could be considered such as MEMS which has been proven to be a great interest of tuning filters because of characteristics such as low loss and excellent linearity.
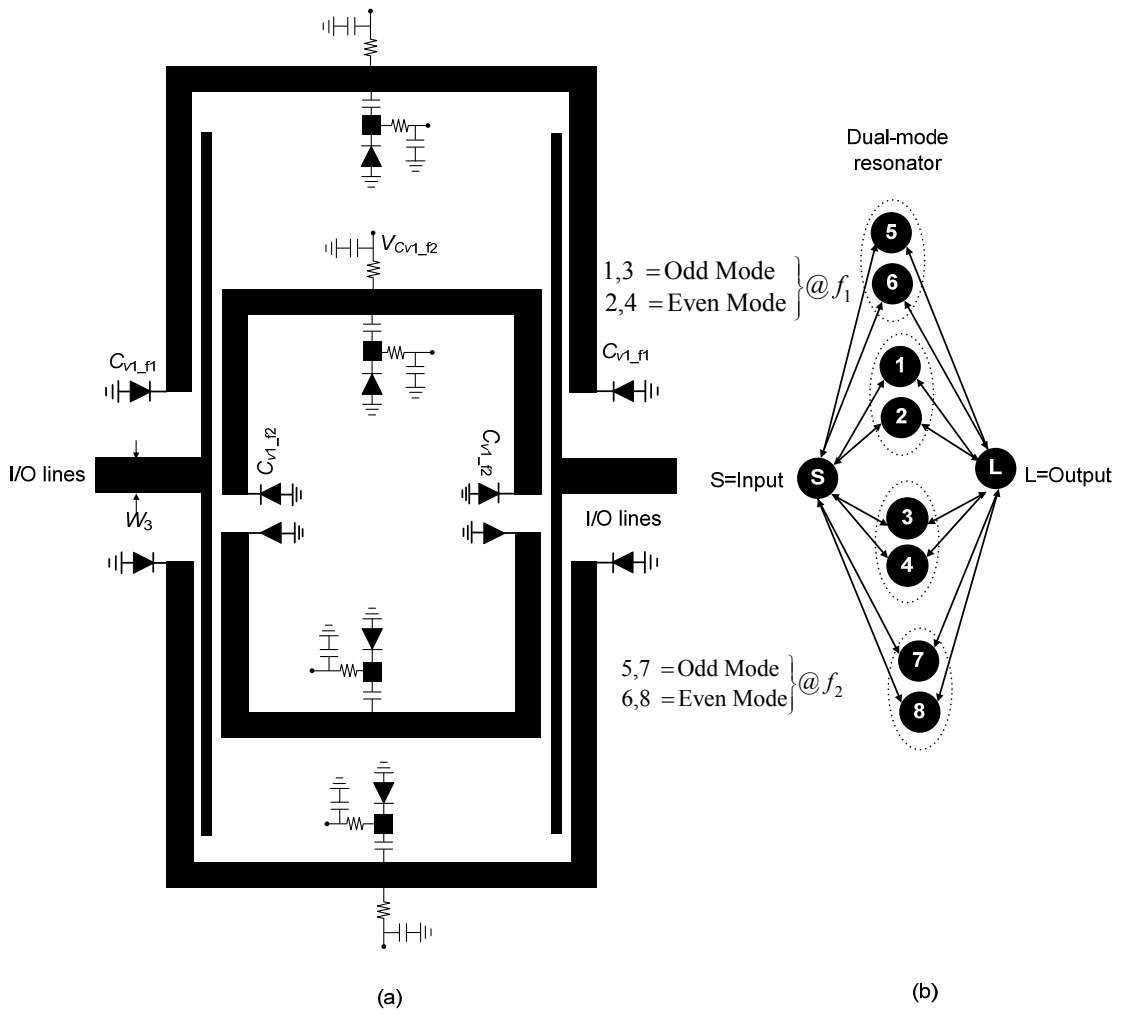
Fig. 6.1. (a) Proposed structure of four-pole dual-band BPF and (b) their coupling structure.

REFERENCES

[1] H. Miyake, S. Kitazawa, T. Ishizaki, T. Yamada, and Y. Nagatomi, "A miniaturized monolothic dual-band filter using ceramic lamination technology for dual mode portable telephones," *IEEE MTT-S Int. Dig. proceeding*, pp. 789-792, 1997.

[2] L. C. Tsai and C. W. Hsue, "Dual-band bandpass filter using equal-length coupled serial-shunted lines and Z-transform Technique," *IEEE Trans. Microw. Theory Tech.*, vol. 52, no. 4, pp. 1111-1117, Apr. 2004.

[3] M. I. Lai and S. K. Jeng, "Compact microstrip dual-band bandpass filters design using genetic-algorithm techniques," *IEEE Trans. Microw. Theory Tech.*, vol. 54, no. 1, pp. 160-168, Jan. 2006.

[4] M. H. Hsu and J. F. Huang, "Annealing algorithm applied in optimization of 2.4 GHz and 5.2 GHz dual-wideband microstrip line filters," *IEICE Trans. Electron.*, vol. E88-C, no. 1, pp. 47-56, Jan. 2005.

[5] J. Lee, M. S. Uhm, and J. H. Park, "Synthesis of self-equalized dual-band filter," *IEEE Microw. Wireless Compon. Lett.*, vol. 15, no. 4, pp. 256-258, Apr. 2005.

[6] J. Lee, M. S. Uhm, and I. B. Yom, "A dual-passband filter of canonical structure for satellite applications," *IEEE Microw. Wireless Compon. Lett.*, vol. 14, no. 6, pp. 271-273, Jun. 2004.

[7] G. Macchiarella and S. Tamiazzo, "Design techniques for dual-passband filters," *IEEE Trans. Microw. Theory Tech.*, vol. 53, no. 11, pp. 3265-3271, Nov. 2005.

[8] R. Cameron, M. Yu, and Y. Wang, "Direct coupled microwave filters with single and dual stop-bands," *IEEE Trans. Microw. Theory Tech.*, vol. 53, no. 11, pp. 3288-3297, Nov. 2005.

[9] J. Lee and K. Sarabandi, "A synthesis method for dual-passband microwave filters," *IEEE Trans. Microw. Theory Tech.,* vol. 55, no. 6, pp. 1163-1170, Jun. 2007.

[10] X. Guan, Z. Ma, P. Chai, Y. Kobayashi, T. Anada, and G. Hagiwara, "Synthesis of dual-band bandpass filters using successive frequency transformations and circuit conversions," *IEEE Microw. Wireless Compon. Lett.*, vol. 16, no. 3, pp. 110-112, Mar. 2006.

[11] X. Guan, Z. Ma, P. Chai, Y. Kobayashi, T. Anada, and G. Hagiwara, "Synthesizing microstrip dual-band bandpass filters using successive frequency transformations and circuit conversations technique," *IEICE Trans. Electron.*, vol. E89-C, no. 4, pp. 495-502, Apr. 2006

[12] X. Guan, Z. Ma, P. Chai, G. Li, Y. Kobayashi, T. Anada, and G. Hagiwara, "A dual-band bandpass filters synthesized by using successive frequency transformations and circuit conversations technique," *IEEE Asia Pacific Microw. Conference proceedings*, pp. 495-502, Dec. 2005.

[13] A. S. Liu, T. Y. Huang, and R. B. Wu, "A dual wideband filter design using frequency mapping and stepped impedance resonators," *IEEE Trans. Microw. Theory Tech.*, vol. 56, no. 12, pp. 2921- 2929, Dec. 2008

[14] H. Joshi and W. J. Chappell, "Dual-band lumped element bandpass filter," *IEEE Trans. Microw. Theory Tech.*, vol. 54, no. 12, pp. 4169-4170, Dec. 2006.

[15] S. G. Mao and M. S. Wu, "Design of artificial lumped-element coplanar waveguide filters with controllable dual-passband responses," *IEEE Trans. Microw. Theory Tech.*, vol. 56, no. 7, pp. 1684-1692, Jul. 2008.

[16] M. Mokhtaari, J. Bornemann, K. Rambabu, and S. Amari, "Coupling matrix design of dual and triple passband filters," *IEEE Trans. Microw. Theory Tech.*, vol. 54, no. 11, pp. 3940-3946, Nov. 2006.

[17] P. Lenoir, S. Bila, F. Seyfert, D. Baillargeat, and S. Verdeyme, "Synthesis and design of asymmetrical dual-band bandpass filter based on equivalent network simplification," *IEEE Trans. Microw. Theory Tech.*, vol. 54, no. 7, pp. 3090-3097, Jul. 2006.

[18] Y. P. Zhang and M. Sun, "Dual-band microstrip bandpass filter using stepped impedance resonators with new coupling scheme," *IEEE Trans. Microw. Theory Tech.*, vol. 54, no. 10, pp. 3779-3785, Oct. 2006.

[19] S. F. Chang, Y. H. Jeng, and J. L. Chen, "Dual-band step impedance bandpass filter for multimode wireless LANs," *Electron. Lett.*, vol. 40, no. 1, pp. 38-39, Jan. 2004.

[20] Q. X. Chu and F. C. Chen, "A compact dual-band bandpass filter using meandering stepped impedance resonators," *IEEE Microw. Wireless Compon. Lett.*, vol. 18, no. 5, pp. 320-322, May 2008.

[21] M. H. Weng, H. W. Wu, and Y. K. Su, "Compact and low loss dual bandpass filter using pseudo-interdigital stepped impedance resonators for WLANs," *IEEE Microw. Wireless Compon. Lett.*, vol. 17, no. 3, pp. 187-189, Mar. 2007.

[22] X. Guan, Z. Ma, P. Cai, T. Anada, and G. Hagiwara, "Design of microstrip dual-band banapass filter with controllable bandwidth," *Microw. Optical Tech. Letters,* vol. 49, no. 3, pp. 740-742, Mar. 2007.

[23] J. Uher and J. R. Hofer, "Tunable microwave and millimeter-wave bandpass filters," *IEEE Trans. Microw. Theory Tech.*, vol. 39, no. 4, pp. 643-653, Apr. 1991.

[24] R. F. Fjerstad, "Some design considerations and realizations of iris-coupled YIG-tuned filters in the 12-40 GHz region," *IEEE Trans. Microw. Theory Tech.,* vol. 18, no .4, pp. 205-212, Apr. 1970.

[25] W. J. Keane, "YIG filters aid wide open receivers," *Microw. J.*, vol. 17, no. 8, pp. 205-212, Sep. 1980.

[26] K. Entesari and G. M. Rebeiz, "A differential 4-bit 6.5-10 GHz RF MEMS tunable filter," *IEEE Trans. Microw. Theory Tech.*, vol. 53, no. 3, pp. 1103-1110, Mar. 2005.

[27] S. Park, M. A. El-Tanani, I. Reines, and G. M. Rebez, "Low-loss 4-6 GHz tunable filter with 3-bit high Q-orthogonal bias RF-MEMS capacitance network," *IEEE Trans. Microw. Theory Tech.*, vol. 56, no. 10, pp. 2348-2355, Oct. 2008.

[28] A. Pothier, J. C. Orlianges, G. Zheng, C. Champeaux, A. Catherinot, P. B. D. Cros, and J. Papaplymerou, " Low-loss 2-bit tunable bandpass filters using MEMS DC contact switches," *IEEE Trans. Microw. Theory Tech.*, vol. 53, no. 1, pp. 354-360, Jan. 2005.

[29] K. Entersari and G. M. Rebeiz, "A 12-18 GHz three-pole RF MEMS tunable filter," *IEEE Trans. Microw. Theory Tech.*, vol. 53, no. 8, pp. 2566-2571, Aug. 2005.

[30] J. Nath, D. Ghosh, J. P. Maria, A. I. Kingon, W. Fathelbab, P. D. Franzon, and M. B. Steer, "An electronically tunable microstrip bandpass filter using thin-film barium-strontium-titante (BST) varactors," *IEEE Trans. Microw. Theory Tech.*, vol. 53, no. 9, pp. 2707-2712, Sep. 2005.

[31] I. Vendik, O. Vendik, V. Pleskachev, A. Svishchev, and R. Wordenweber, "Design of tunable ferroelectric filters with a constant fractional bandwidth," *IEEE MTT-S Int. Microw. Symp. Dig.*, pp. 1461-1464, 2001.

[32] L. H. Hsieh and K. Chang, "Tunable microstrip bandpass filters with two transmission zeros," *IEEE Trans. Microw. Theory Tech.*, vol. 51, no. 2, pp. 520-525, Feb. 2003.

[33] B. Liu, F. Wei, and X. Shi, "Reconfigurable bandpass filter based on net-type stepped impedance resonator," *Electronics Letters*, vol. 46, no. 22, pp. 1506-1507, Feb. 2010.

[34] I. C. Hunter and J. D. Rhodes, "Electronically tunable microwave band pass filters," *IEEE Trans. Microw. Theory Tech.*, vol. 30, no. 9, pp. 1354-1360, Sep. 1982.

[35] B. W. Kim and S. W. Yun, "Varactor tuned combline bandpass filter using step-impedance microstrip lines," *IEEE Trans. Microw. Theory Tech.*, vol. 52, no. 4, pp. 1279-1283, Apr. 2004.

[36] A. R. Brown and G. M. Rebeiz, "A varactor tuned RF filter," *IEEE Trans. Microw. Theory Tech.*, vol. 48, no. 7, pp. 1157-1160, Jul. 2000.

[37] S. J. Park and G. M. Rebeiz, "Low loss two pole tunable filters with three different predefined bandwidth characteristics," *IEEE Trans. Microw. Theory Tech.,* vol. 56, no. 5, pp. 1137-1148, May 2008.

[38] W. Tang and J. Hong, "Varactor-tuned dual-mode bandpass filters," *IEEE Trans. Microw. Theory Tech.*, vol. 58, no. 8, pp. 2213-2219, Aug. 2010.

[39] J. Long, C. Li , W. Cui, J. Huangfu, and L. Ran, "A tunable microstrip bandpass filter with two independently adjustable transmission zeros," *IEEE Microw. Wireless Compon. Letters*, vol. 21, no. 2, pp. 74-76, Feb. 2011.

[40] Y. Chiou and G. M. Rebeiz, "A tunable three-pole 1.5-2.2 GHz bandpass filter with bandwidth and transmission zero control," *IEEE Trans. Microw. Theory Tech.,* vol. 59, no. 11, pp. 2872-2878, Nov. 2011.

[41] H. Jiang, B. Lacroix, K Choi, Y. Wang, A. T. Hunt and J. Papapolymerou, "*Ka*- and *U*-band tunable bandpass filters using ferroelectric capacitors," *IEEE Trans. Microw. Theory Tech.,* vol. 59, no. 12, pp. 3068-3074, Dec. 2011.

[42] S. Moon, H. H. Sigmarsson, H. Joshi, and W. J. Chappell, "Substrate integrated evanescent-mode cavity filter with a 3.5 to 1 tuning ratio," *IEEE Microw. Wireless Compon. Letters*, vol. 20, no. 8, pp. 450-452, Aug. 2010.

[43] X. Y. Zhang and Q. Xue, "Novel centrally loaded resonators and their applications to bandpass filters," *IEEE Trans. Microw. Theory Tech.*, vol. 56, no. 4, pp. 913-921, Apr. 2008.

[44] D. Girbau, A. Lazaro, E. Martinez, D. Masone, and L. Pradell, "Tunable dual-band bandpass filter for WLAN applications," *Microw. Optical Tech. Letts.*, vol. 51, no. 9, pp. 2025-2028, Sep. 2009.

[45] Y. Chiou and G. M. Rebeiz, "A quasi elliptic function 1.75-2.25 GHz 3-pole bandpass filter with bandwidth control," *IEEE Trans. Microw. Theory Tech.*, vol. 60, no. 2, pp. 244-249, Feb. 2012.

[46] E. E. Djoumessi, M. Chaker, and K. Wu, "Varactor-tuned quarter-wavelength dual-bandpass filter," *IET Microw. Antenna and Propagation,* vol. 3, no. 1, pp. 117-124, Feb. 2009.

[47] A. L. C. Serrano, F. S. Correra, T. P. Vuong, and P. Ferrari, "Synthesis methodology applied to a tunable path filter with independently frequency and bandwidth control," *IEEE Trans. Microw. Theory Tech*., vol. 60, no. 3, pp. 484-493, Mar. 2012.

[48] M. Sanchez-Renedo, R. Gomez-Garcia, J. I. Alonso, and C. Briso-Rodriguez, "Tunable combline filter with continuous control of center frequency and bandwidth," *IEEE Trans. Microw. Theory Tech.*, vol. 53, no. 1, pp. 191-199, Jan. 2005.

[49] C. C. Cheng and G. M. Rebeiz, "High-Q 4-6 GHz suspended stripline RF MEMS tunable filter with bandwidth control," *IEEE Trans. Microw. Theory Tech.,* vol. 59, no. 10, pp. 2469-2476, Oct. 2011.

[50] X. Y. Zhang and Q. Xue, "High selectivity tunable bandpass filters with harmonic suppression," *IEEE Trans. Microw. Theory Tech.,* vol. 58, no. 4, pp. 964-969, Apr. 2010.

[51] G. Matthaei, L. Young, and E. M. T. Jones, *Microwave Filters, Impedance-matching Networks and Coupling Structures*, McGraw-Hill Book Co., New York, NY 1964.

[52] J. Lim, S. Oh, J. Koo, Y. Jeong, and D. Ahn, "A power divider with adjustable dividing ratio," *IEICE Trans. Electron*, vol. E91-C, no. 3, pp. 389-391, Mar. 2008.

[53] D. Ahn, J. Park, C. Kim, J. Kim, Y. Qian, and T. Itoh, "A design of the low-pass filter using a novel microstrip defected ground structure," *IEEE Trans. Microw. Theory Tech.*, vol. 49, no. 1, pp. 86-93, Jan. 2001.

[54] J. Lim, J. Lee, J. Lee, S.-M. Han, D. Ahn, and Y. Jeong, "A new calculation method for the characteristic impedance of transmission lines with modified ground structure or perturbation," *Progress in Electrom. Research*, vol. 106, pp. 147-162, 2010.

[55] S. Sun and L. Zhu, "Periodically non-uniform coupled microstrip-line filter with harmonic suppression using transmission zero reallocation," *IEEE Trans. Microw. Theory Tech.*, vol. 53, no. 5. pp. 1817-1822, May 2005.

[56] J. S. Lim, S. W. Lee, C. S. Kim, J. S. Park, D. Ahn, and S. Nam, "A 4:1 unequal Wilkinson power divider," *IEEE Microw. Wireless Compon. Letters*, vol. 11, no.3, pp. 124-126, Mar. 2001.

[57] Y. Jeong, S. Jeong, J. Lim and S. Nam, "A new method to suppress harmonics using $\lambda/4$ bias line combined by defected ground structure in power amplifier," *IEEE Microw. Wireless Compon. Letters*, vol. 13, no. 12, pp. 538-540, Dec. 2001.

[58] J. Park, J. Kim, and S. Nam, "Design of a novel harmonic suppressed microstrip low-pass filter," *IEEE Microw. Wireless Compon. Letters,* vol. 17, no. 6, pp. 424-426, Jun. 2007.

[59] D. Woo and T. Lee, "Suppression of harmonics in Wilkinson power divider using dual-band rejection by asymmetric DGS," *IEEE Trans. Microw. Theory Tech.*, vol. 53, no. 6, pp. 2139- 2144, Jun. 2005.

[60] C. Kim, D. Kim, I. Song, K. Leong, T. Itoh, and D. Ahn, "A design of a ring bandpass filters with wide rejection band using DGS and spur-line coupling structures," *in IEEE MTT-S Int. Microw. Symp. Dig.*, pp. 2183-2186, 2005.

[61] J. Lim, C. Kim, D. Ahn, Y. Jeong, and S. Nam, "Design of low-pass filters using defected ground structure," *IEEE Trans. Microw. Theory Tech.*, vol. 53, no. 8, pp. 2539-2545, Aug. 2005.

CURRICULUM VITAE

Girdhari Chaudhary

#7304, Division of Electronics and Information Engineering, Chonbuk National University, 567 Baeje-daero, Jeonju-si, Chollabuk-do, 561-756, Republic of Korea

Mobile Phone : +82-17-654-858

E-mail : girdharichaudhari@gmail.com, girdharic@jbnu.ac.kr

RESEARCH INTERESTS

I have worked on **multi-band passive circuits design, mostly on multi-band filters.** I have a rich experience in circuit and system design through simulation, implementation and measurement. And now I would like to broaden my knowledge to the transmitting and receiving front-end integrated circuit design including CMOS RFIC, especially to the development of next generation transistor device.

EDUCATION

Ph.D., Electronic and Information Engineering, *Chonbuk National University* Academic Advisor : Professor Yongchae Jeong	2009-present
M.Tech., Electronics and Communication Engineering, *Malaviya National Institute of Technology (MNIT),* Jaipur, India	2005-2007
B.E., Electronic and Communication Engineering, *Nepal Engineering College, Pokhara University, Nepal*	2000-2004

AWARDS AND HONORS

Outstanding performance in academic publications for second stage of BK21 fostering a world class talent selected the Ministry of Education, Science and Technology, South Korea (Chonbuk National University	2012

Advanced Graduated Education Center of Jeonbuk for Electronics and Information Technology-BK21)	
Best Paper Award (sponsored by the Korean Institute of Electromagnetic Engineering Science) "A tunable dual-band bandpass filter design using variable characteristic impedance transmission lines"	2011
Electronics Award (sponsored by Nepal Engineering College, Pokhara University (PU), Nepal)	2003
Mathematics Award (sponsored by Nepal Engineering College, Pokhara University (PU), Nepal)	2002

REFERENCES

Yongchae Jeong, Ph.D

Professor, Academic Advisor (*Senior Member, IEEE*)

#7304, Division of Electronics and Information Engineering,

Chonbuk National University, 664-14,

567 Baekje-daero, Jeonju-si, Chollabuk-do, 561-756, Republic of Korea

Phone   : +82-63-270-2458

Fax   : +82-63-270-2394

E-mail   : ycjeong@jbnu.ac.kr

Jongsik Lim, Ph.D

Associate Professor, (*Senior Member, IEEE*)

Department of Electrical and Communication Engineering,

Soonchunhyang University, Eupnae-ri,

Shinchang-myeon, Asan-si, Choongnam, 336-745, Republic of Korea

Phone   : +82-41-530-1332

Fax   : +82-41-530-1548

E-mail   : jslim@sch.ac.kr

PUBLICATION

INTERNATIONAL PEER-REVIEWED JOURNALS

[1] **Girdhari Chaudhary**, Yongchae Jeong, and Jongsik Lim, "A broad-bandwidth dual-band bandpass filter design using composite right/left handed transmission lines," *Journal of Electromag. Waves and Applications,* vol. 25, pp. 2138-2147, 2011.

[2] **Girdhari Chaudhary**, Heungjae Choi, Yongchae Jeong, Jongsik Lim, Dongsu Kim and Jun-Chul Kim, "Design of dual-band bandpass filter using DGS with controllable second passband," *IEEE Microw. Wireless Compon. Lett.,* vol. 21, no. 11, pp. 589-591, Nov. 2011.

[3] **Girdhari Chaudhary**, Yongchae Jeong, Kwisoo Kim and Dal Ahn, "Design of dual-band bandpass filters with controllable bandwidths using new mapping function," *Progress in Electromag. Research,* vol. 124, pp. 17-34, Jan. 2012.

[4] **Girdhari Chaudhary** and Y. Jeong, "Design of vector modulator using low phase deviation attenuators with large amplitude variations range," *Journal of Electromag. Waves and Applications,* vol. 26, pp. 402-410, 2012.

[5] **Girdhari Chaudhary**, Heungjae Choi, Yongchae Jeong, Jongsik Lim and Chul-Dong Kim, "Design of group delay time controller based on a reflective parallel resonator," *ETRI Journal,* vol. 34, no. 2, pp. 210-215, Apr. 2012.

[6] **Girdhari Chaudhary**, Yongchae Jeong, and Jongsik Lim, "Harmonic suppressed dual-and bandpass filters with tunable passbands," *IEEE Trans. Microw. Theory Tech.*, vol. 60, no. 7, pp. 2115-2123, Jul. 2012.

[7] **Girdhari Chaudhary**, Phirun Kim, Yongchae Jeong, and Jae-Hun Yoon, "Design of high efficiency RF-DC conversion circuit using novel termination networks for RF energy harvesting system," *Microw. Opt. Technol. Lett.,* vol. 54, no. 10, pp. 1729-1732, Oct. 2012.

[8] Yongchae Jeong, **Girdhari Chaudhary,** and Jongsik Lim, "A dual-band high efficiency class-F GaN power amplifier using a novel harmonic-rejection load network," *IEICE Trans. Electronics*., vol. E95-C, no. 11, pp. 1783-1789, Nov. 2012.

[9] **Girdhari Chaudhary,** Yongchae Jeong, and Jongsik Lim, "Dual-band bandpass filter with independently tunable center frequencies and bandwidths," accepted for publication in *IEEE Trans. Microw. Theory Tech*., vol. 61, no. 1, Jan. 2013.

INTERNATIONAL CONFERENCE PRESENTATIONS

[1] **Girdhari Chaudhary**, Yongchae Jeong, Jongsik Lim, Chul -Dong Kim, Jun-Chul Kim, and Jong-Chul Park, "DMS harmonic termination load network for high efficiency power amplifier applications," *Proc. of 40th European Microw. Conf.*, pp.765-768, 2010.

[2] Heungjae Choi, **Girdhari Chaudhary**, Younggyu Kim, Yongchae Jeong, and Chul-Dong Kim, "Characterization of the power amplifier group delay by using predistortive cancellation technique," *Proc. 40th Eur. Microw. Conf.*, pp. 1014-1017, 2010.

[3] Younggyu Kim, Sungun Shim. Taesu Moon, **Girdhari Chaudhary**, and Yongchae Jeong, "Mathematical analysis of novel low phase deviation variable attenuator," *Proc. Asia-Pacific Microw. Conf.*, pp. 1743-1746, 2010.

[4] Heungjae Choi, **Girdhari Chaudhary**, Taesu Moon, Yongchae Jeong, Jongsik Lim, and Chul-dong kim, "A design of composite negative group delay circuit with lower signal attenuation for performance improvement of power amplifier linearization techniques," *IEEE MTT-S Int. Microw. Symp. Dig.*, 2011.

[5] **Girdhari Chaudhary**, Phirun Kim, Yongchae Jeong, Jongsik Lim and Jaehoon Lee, "Analysis and circuit modeling method for defected microstrip structure in planar transmission lines," *Proc. Asia-Pacific Microw. Conf.*, pp. 999-1002, 2011.

[6] **Girdhari Chaudhary**, Sungdoo Park, Yongchae Jeong, Jongsik Lim and Jun Lee, "A tunable group delay circuit for time delay matching applications in communication systems," *Proc. Asia-Pacific Microw. Conf.*, pp. 1170-1173, 2011.

[7] **Girdhari Chaudhary**, Phirun Kim, Yongche Jeong, and Jongsik Lim, "Dual-mode bandpass filter with independently tunable center frequency and bandwidth," *Proc. IEEE Radio-frequency integration technology symposium*, pp. 56-58, 2012.

[8] Junhyung Jeong, Sungdoo Park, **Girdhari Chaudhary**, and Yongchae Jeong, "Design of tunable negative group delay circuit for communication systems," *Proc. IEEE Radio-frequency integration technology symposium*, pp. 59-61, 2012.